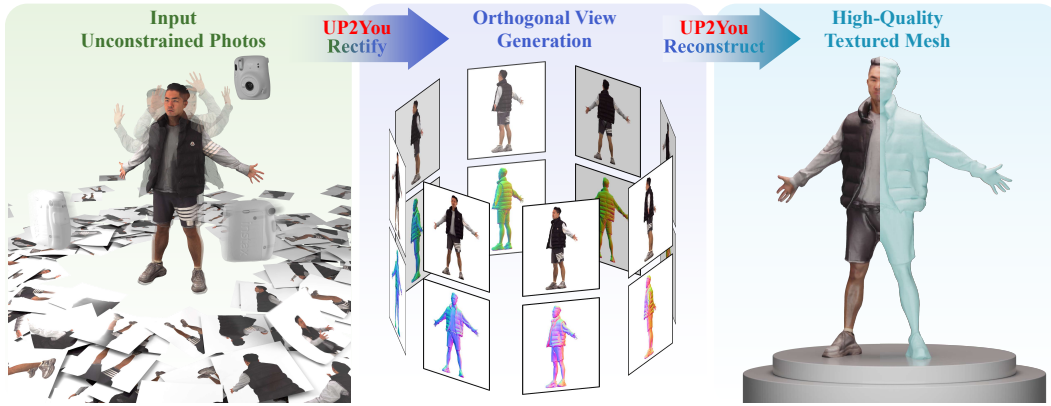


000 UP2YOU: FAST RECONSTRUCTION OF YOURSELF 001 FROM UNCONSTRAINED PHOTO COLLECTIONS 002

003 **Anonymous authors**

004 Paper under double-blind review



005
006
007
008
009
010
011
012
013
014
015
016
017
018
019
020
021
022
023
024
025
026
027
028
029
030
031
032
033
034
035
036
037
038
039
040
041
042
043
044
045
046
047
048
049
050
051
052
053
Figure 1: Overview of UP2You. Our method reconstructs high-quality, textured 3D clothed portraits from unconstrained photo collections. It robustly handles highly diverse and unstructured inputs by rectifying them into orthogonal multi-view images and corresponding normal maps, making them compatible with traditional reconstruction algorithms.

ABSTRACT

We present UP2You, the first tuning-free solution for reconstructing high-fidelity 3D clothed portraits from extremely unconstrained in-the-wild 2D photos. Unlike previous approaches that require “clean” inputs (e.g., full-body images with minimal occlusions, or well-calibrated cross-view captures), UP2You directly processes raw, unstructured photographs, which may vary significantly in pose, viewpoint, cropping, and occlusion. Instead of compressing data into tokens for slow online text-to-3D optimization, we introduce a *data rectifier* paradigm that efficiently converts unconstrained inputs into clean, orthogonal multi-view images in a single forward pass within seconds, simplifying the 3D reconstruction. Central to UP2You is a pose-correlated feature aggregation module (PCFA), that selectively fuses information from multiple reference images w.r.t. target poses, enabling better identity preservation and nearly constant memory footprint, with more observations. We also introduce a perceiver-based multi-reference shape predictor, removing the need for pre-captured body templates. Extensive experiments on 4D-Dress, PuzzleIOI, and in-the-wild captures demonstrate that UP2You consistently surpasses previous methods in both geometric accuracy (Chamfer-15%↓, P2S-18%↓ on PuzzleIOI) and texture fidelity (PSNR-21%↑, LPIPS-46%↓ on 4D-Dress). UP2You is efficient (1.5 minutes per person), and versatile (supports arbitrary pose control, and training-free multi-garment 3D virtual try-on), making it practical for real-world scenarios where humans are casually captured. Both models and code will be released to facilitate future research on this underexplored task.

1 INTRODUCTION

Reconstructing 3D clothed humans from **unconstrained photo collections**, like the personal albums (Fig. 2-Left), is a challenging and largely unexplored research frontier. Unlike prior tasks such as single-image 3D reconstruction [23, 48, 65, 92, 93], monocular video-based reconstruction [18, 28, 35], or multi-view 3D reconstruction [55, 64, 101], this problem is distinguished by the highly unstructured nature of the input: appearance information is present but scattered across photos where subjects are often partially captured or occluded, and camera as well as body poses are rarely synchronized. As a result, establishing accurate 2D-to-3D correspondences is extremely difficult,

even with the help of most advanced off-the-shelf human-centric estimators (i.e., camera, body pose, landmarks, geometric cues, etc). In contrast, traditional 3D reconstruction algorithms typically assume “clean captures” (i.e., full-body capture with simple poses, synchronized cameras, etc), where well-aligned 2D-to-3D correspondences can be readily established using the estimators above.

Two potential strategies to address above challenges: **1) Data Compressor**: Crop and group photos into local and global patches (e.g., head, full-body) [102], or segment input photos into multiple assets (e.g., garments, hair, face, accessories) [94], then compress these patches or assets into learnable tokens, and finally assemble them as text prompt to generate 3D humans via text-to-3D techniques [62]; **2) Data Rectifier**: Convert the incoming “dirty or incomplete captures” into clean and complete ones, e.g., orthogonal orbit views with canonical poses, which are easier to reconstruct with traditional 3D reconstruction algorithms. Essentially, the data compressor operates mainly at the representation level, without substantially improving the generative model’s ability to ensure 3D consistency and identity preservation — a limitation noted in PuzzleAvatar [94] as “unpredictable hallucination.” The data rectifier, however, refines not only the input data but also the generative model’s prior, via continued training on synthetic multi-view renderings of high-fidelity 3D clothed humans, enabling more consistent 3D reconstruction in terms of both identity and viewpoint, from unconstrained photographs. UP2You falls in the second category, as shown in Fig. 2.

PuzzleAvatar [94] is the representative of the first strategy, it first “decompose” the unconstrained photos into multiple asset soups, all of which are linked with unique learned tokens via DreamBooth [70], then it “compose” these assets into a 3D full-body representation via score-distillation sampling (SDS) [62], where the 3D reconstruction task is reformulated as a text-to-3D task, bypassing explicit canonicalization. However, this process takes hours since both DreamBooth fine-tuning and SDS-based optimization are time-consuming and unstable, see Fig. 2. Additionally, ground-truth SMPL-X meshes are needed for initialization, as predicting shape parameters from unconstrained photo collections is non-trivial. Regarding the second strategy — converting inputs into orthogonal orbit views — some attempts [23, 48, 60] have been made. However, these methods are restricted to single-image inputs and cannot fully leverage the multiple unconstrained photos. Essentially, these methods act more as “data inpainters” [84] — synthesizing unseen views from seen capture — rather than as “data rectifiers” that unify the messy observations into structured output. Designed mainly for constrained inputs (i.e., a single image with full-body coverage), these methods cannot handle unconstrained photos or scale up the reconstruction accuracy with the number of inputs.

To the best of our knowledge, UP2You is the first work to unlock the “data rectifier” strategy on unconstrained photo collections, directly transforming raw unconstrained photo collections into orthogonal views while faithfully preserving subject identity. This is not a trivial extension of prior arts, as it 1) requires effectively aggregating information from multiple unconstrained inputs, which may vary significantly in terms of body poses, camera viewpoints, cropings, and occlusions; 2) must be efficient enough to process varying numbers of input photos (ranging from one to dozens) without incurring significant computational overhead; and 3) needs to overcome the dependency on ground-truth body shapes, which are often unavailable in real-world scenarios.

Specifically, UP2You aggregates ReferenceNet features [27], extracted from unconstrained photos according to body poses, via the proposed Pose-Correlated Feature Aggregation (PCFA) module. This module implicitly learns correlation weights between unconstrained reference images and target pose conditions (i.e., SMPL-X normal maps). Guided by these correlation maps, PCFA uses an optimized `topk` strategy to selectively aggregate the most informative image features for generating each orthogonal view. As a result, the memory footprint remains nearly constant regardless of the number of input photos, enabling effective and efficient information fusion.

To get rid of the dependence on ground-truth body shapes, we design a shape predictor based on perceiver structure [34, 46] to regress SMPL-X shape parameters directly from unconstrained photo collections. Lastly, with another MV-Adapter [32] to generate multi-view normal maps, followed by mesh carving and texture baking [48], UP2You reconstructs high-quality textured meshes from unconstrained photos in 1.5 minutes. We evaluate our generation results on PuzzleIOI, 4D-Dress, and self-collected in-the-wild datasets. Our method surpasses other state-of-the-art approaches in both geometric accuracy (Chamfer-15%↓, P2S-18%↓ on PuzzleIOI) and texture fidelity (PSNR-21%↑, LPIPS-46%↓ on 4D-Dress), while also demonstrating flexibility and superior generalization for single-image reconstruction, and enabling 3D virtual try-on application, all without extra training.

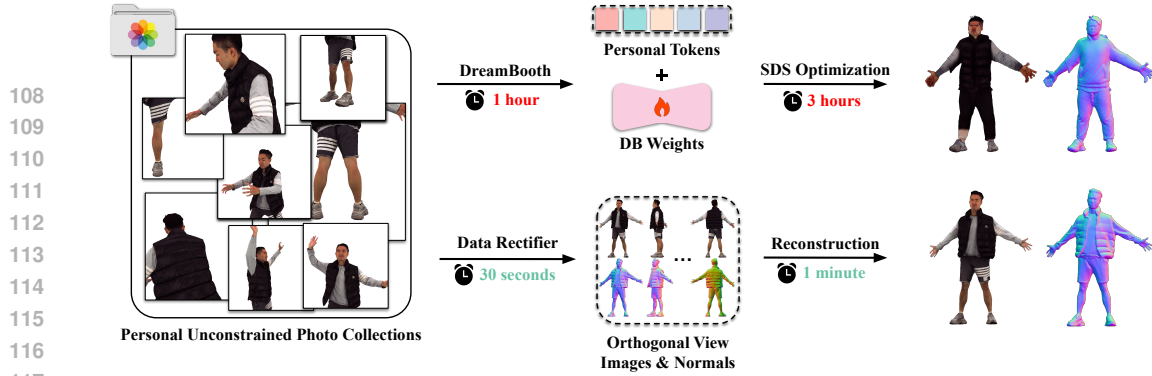


Figure 2: **Paradigm differences between previous works and UP2You.** **Top:** Previous works like PuzzleAvatar [94] and AvatarBooth [102] compress unconstrained photos into implicit personal tokens and DreamBooth weights [70] through fine-tuning, then generate 3D humans via SDS optimization [70]. **Bottom:** UP2You directly rectifies unconstrained photo collections into orthogonal view images and normals, then reconstructs textured human meshes, achieving superior quality while reducing processing time from 4 hours to 1.5 minutes.

Our main contributions w.r.t. the prior arts are as follows:

- **Efficient.** As Fig. 2 shows, unlike previous DreamBooth + SDS paradigm (>4 hours), UP2You acts as a “data rectifier” instead, to directly generate “clean” multi-views from “dirty” unconstrained inputs in one forward pass (<15 secs). It can process one, several, or dozens of photos with a nearly constant memory footprint. The full pipeline, including multi-view normal generation plus mesh carving and texture baking, completes in 1.5 minute.
- **Effective.** Thanks to the PCFA module, which selectively aggregates the most informative regions from the reference images for synthesizing target views, UP2You significantly outperforms prior SOTAs (PuzzleAvatar, AvatarBooth, PSHuman) in both geometry accuracy and texture fidelity, and delivers consistent shape and identity regardless of input forms or pose conditions. Notably, the reconstruction quality even scales up with more unconstrained inputs, echoing the principle of *The More You See in 2D, the More You Perceive in 3D* [21].
- **Versatile.** PuzzleAvatar requires an A-posed body template with ground-truth shape for 3D initialization, while UP2You is flexible to random pose control, directly regresses body shapes from unconstrained photos, and inherently supports multi-garment 3D virtual try-on, for free.

2 RELATED WORK

2.1 3D CLOTHED HUMAN RECONSTRUCTION

The field of 3D clothed human reconstruction has been extensively studied over the past few decades. Early methods primarily focused on reconstructing human geometry and texture from dense multi-view image captures [35, 52, 61]. Subsequent research has broadened the scope to include full-shot monocular video inputs [18, 19, 28, 90], enabling more flexible and accessible data acquisition. Recent advances in generative models, particularly diffusion models [25, 42, 69, 81], and the emergence of SDS-based 3D human generators [30, 44, 50, 53, 86, 86], have further propelled the field. An increasing number of video-based human reconstruction approaches now leverage learned generative priors to address common challenges in real-world video captures, such as occlusions [19, 59], view inconsistencies [36], and poor texture details [83].

Such generative priors, learned from large-scale datasets, play a more crucial role for the inherently ill-posed problem of 3D human reconstruction, especially when the input data is sparse or incomplete. The most sparse input format is a single image [23, 31, 33, 48, 65, 67, 71, 72, 92, 93, 107]. In essence, it can be regarded as a “conditional generation” problem [31], since large portions of the geometry — such as the unseen backside and occluded regions — must be plausibly inferred or synthesized from the visible pixels. Building on this “reconstruction as conditional generation” paradigm, numerous works have further advanced the field [3, 15, 48, 105]. Apart from multi-view posed captures, full-shot monocular video, and single image, numerous works have sought to expand the range of input modalities, for example, by incorporating dual front-back captures [38, 55] or multi-view unposed full-body images [29, 66, 97, 101, 108] to improve reconstruction fidelity and completeness.

Despite these advances, existing methods still fall short of handling truly “unconstrained” photos — those with partial views, occlusions, extreme camera viewpoints, dynamic body poses, and inconsistent aspect ratios. Accurately estimating body shape [12, 43, 45, 89, 98, 104] from such

unconstrained photo collections is nearly impossible. Moreover, given multiple “dirty” reference images, image-based HMR methods often fail to deliver consistent results. This inconsistency manifests as significant variations in the predicted body shapes for the same subject — some reconstructions may appear unnaturally thin, others excessively fat, and some may completely fail, especially in cases of partial or occluded inputs. As shown in Tab. 2 and Fig. 7, it becomes challenging to determine which, if any, of the predicted shapes truly represent the subject.

In contrast, UP2You addresses these data format constraints by functioning as a comprehensive “data rectifier,” directly transforming unstructured or “dirty” inputs into orthogonal “clean” views, with consistent 3D and identity, that can be seamlessly utilized for robust 3D reconstruction.

2.2 UNCONSTRAINED PHOTOS TO 3D

Most real-world data is inherently unstructured, presenting significant challenges for 3D reconstruction tasks that require reliable spatial correspondences. The earliest work in “Unconstrained Photos to 3D” can be traced back to Photo Tourism [80], which reconstructs 3D scenes from large collections of Internet photos. Recent advances in neural rendering and generative models have further advanced this field, enabling more robust and realistic 3D reconstructions from unstructured image collections [10, 49, 87]. However, these methods primarily focus on rigid objects or scenes and cannot be directly applied to 3D clothed human reconstruction, which involves highly articulated and non-rigid structures. A critical open question is how to effectively extract and aggregate identity features from unconstrained photos — not only for general objects [41, 103, 109], but especially for dynamic humans — and reproduce them in a 3D-consistent manner. Several works on subject-driven image generation [2, 4, 13, 14, 16, 40, 70, 73, 85], as well as ID-consistent 2D human portrait generation [9, 63, 75, 84, 95], are discussed in the *Sup.Mat.* (Appendix B). However, these methods are primarily designed for 2D image generation and lack the mechanisms to ensure cross-view consistency or the precise latent feature aggregation necessary for high-fidelity 3D reconstruction.

The most relevant works addressing this challenge are PuzzleAvatar [94] and AvatarBooth [102]. Both first employ few-shot personalization [4, 70], as Total Selfie [9] and RealFill [84], to distill identity information from unconstrained photos into a customized diffusion model, as unique tokens. Subsequently, guided by these unique tokens, they utilize Score Distillation Sampling (SDS) [7, 37, 62, 100] to optimize a neural-based 3D representation [56, 76]. In short, the entire pipeline of these methods can be summarized as “unconstrained photos → personalized diffusion models with learned specialized tokens → SDS-based Text-to-3D”. However, fine-tuning diffusion models and optimization-based SDS methods are extremely time-consuming. Moreover, these fine-tuning approaches act as a form of lossy compression: the strong priors of diffusion models often override subject-specific features, leading to a loss of identity and fine-grained details, or even introducing unpredictable hallucinations. In contrast, UP2You is a tuning-free method that faithfully reconstructs 3D humans from unconstrained photos in just 1.5 minutes, while well preserving human identities.

3 METHOD

Our objective is to reconstruct a high-quality textured mesh from unconstrained photos with unknown camera parameters and human poses. To this end, we first generate orthogonal full-body images from the unconstrained inputs, conditioned on SMPL-X normal maps that contain both camera and pose information (Sec. 3.1). Next, we utilize these orthogonal multi-view RGB images to generate corresponding multi-view normal maps, which serve as geometric cues for detailed mesh reconstruction (Sec. 3.2). To handle in-the-wild images without SMPL-X annotations, we further introduce a body shape estimator capable of inferring human body shape by integrating information from a handful of unconstrained photos (Sec. 3.3).

3.1 ORTHOGONAL MULTI-VIEW IMAGES GENERATION

To tackle orthogonal multi-view image generation from unconstrained photo collections, we adopt MV-Adapter [32] as our backbone (introduced in Appendix C). MV-Adapter integrates ReferenceNet \mathcal{R} [27] as the reference image encoder and incorporates raymaps into the diffusion UNet as view conditions, enabling the synthesis of six orthogonal views. For our task, we use orthogonal SMPL-X

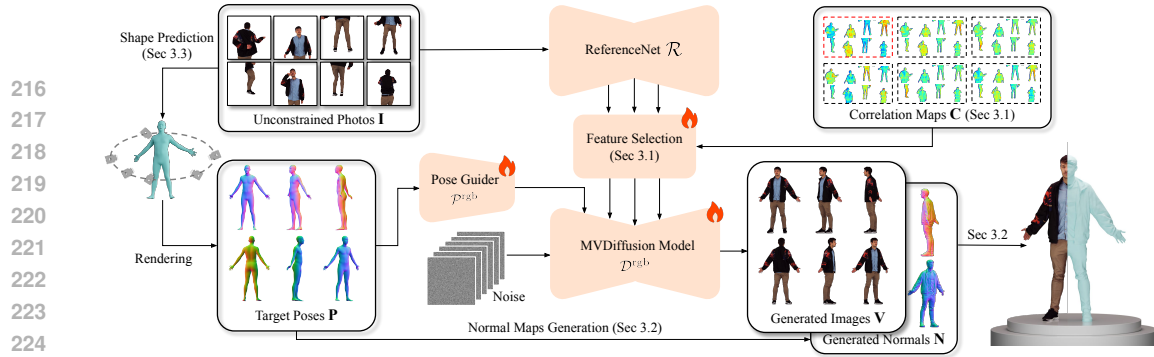


Figure 3: **Pipeline of UP2You.** Given unconstrained input photos \mathbf{I} , we first predict the SMPL-X shape parameters (Sec. 3.3) and initialize the SMPL-X mesh with predefined pose and expression parameters. We then generate orthogonal view images \mathbf{V} based on \mathbf{I} and SMPL-X normal rendering \mathbf{P} with the proposed PCFA method—predict correlation maps \mathbf{C} and select most informative features (Sec. 3.1). Finally, we produce multi-view normal maps \mathbf{N} from \mathbf{P} and \mathbf{V} , and reconstruct the final textured mesh (Sec. 3.2).

normal maps as view conditions. Unlike the original MV-Adapter, which handles only single-image inputs, our approach extends it to process multiple unconstrained photos.

As shown in Fig. 3, given N unconstrained reference images $\mathbf{I} = \{\mathbf{I}_1, \dots, \mathbf{I}_N\}$ of a person in the same outfit, our goal is to synthesize M orthogonal target views $\mathbf{V} = \{\mathbf{V}_1, \dots, \mathbf{V}_M\}$, each conditioned on a corresponding SMPL-X normal map $\mathbf{P} = \{\mathbf{P}_1, \dots, \mathbf{P}_M\}$. To extract the most informative features for each target view, we introduce the Pose-Correlated Feature Aggregation (PCFA) module, which predicts correlation maps $\mathbf{C} = \{\mathbf{C}_1^i, \dots, \mathbf{C}_N^i\}_{i=1}^M$ between reference and target views (see Fig. 4). Based on \mathbf{C} , PCFA select features for each target viewpoint for the generation of orthogonal views \mathbf{V} .

Correlation Map Prediction. Using all reference features for ortho-view generation is computationally intensive, as memory usage grows with the number of unconstrained references. However, many reference pixels are irrelevant for a given target view (e.g., back-view references for front-view synthesis). Therefore, we adaptively determine each reference’s contribution based on the target pose to reduce computational cost.

To achieve this, we disentangle human-specific identity features from viewpoint correlation information in the unconstrained reference inputs. Drawing inspiration from [26, 39], we predict correlation maps for reference images conditioned on target poses, as illustrated in Fig. 4. For each target pose $\mathbf{P}_i, i \in \{1, 2, \dots, M\}$, we estimate a correlation map that indicates the pixel-wise relevance of each reference image for generating the corresponding view. Specifically, we employ a pose image encoder $\mathcal{E}^{\text{pose}}$ and a DINOv2 [57] model \mathcal{E}^{ref} to extract features from the target pose image and all reference images: $\mathbf{X}_i^{\text{pose}} = \mathcal{E}^{\text{pose}}(\mathbf{P}_i)$ and $\mathbf{X}^{\text{ref}} = \mathcal{E}^{\text{ref}}(\mathbf{I})$, where \mathbf{X}^{ref} represents the concatenation of all DINOv2 outputs $\{\mathbf{X}_j^{\text{ref}}\}_{j=1}^N$. Subsequently, we feed both $\mathbf{X}_i^{\text{pose}}$ and \mathbf{X}^{ref} into a transformer block \mathcal{T} that comprises layers of self-attention and cross-attention, where $\mathbf{X}_i^{\text{pose}}$ functions as the *query*, *key*, and *value* in self-attention operations, and as the *query* in cross-attention operations, while \mathbf{X}^{ref} serves as both *key* and *value* in cross-attention operations. Through \mathcal{T} , an output feature $\mathbf{O}_i = \mathcal{T}(\mathbf{X}_i^{\text{pose}}, \mathbf{X}^{\text{ref}})$ that integrates reference information relevant to the target pose is produced. We derive the image correlation map \mathbf{C}^i by computing the attention map between \mathbf{O}_i and \mathbf{X}^{ref} :

$$\mathbf{A}^i = \frac{\mathcal{W}_q \mathbf{O}_i \times \mathcal{W}_k \mathbf{X}^{\text{ref}} \top}{\sqrt{d}}, \quad (1)$$

$$\begin{aligned} \mathbf{C}^i &= [\mathbf{C}_1^i, \mathbf{C}_2^i, \dots, \mathbf{C}_N^i] \\ &= \text{ReLU}(\text{AvgPool}(\text{mean}(\mathbf{A}^i))), \end{aligned} \quad (2)$$

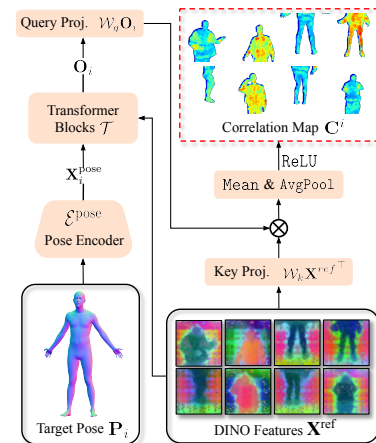


Figure 4: **Pose-Dependent Correlation Map.** Correlation is colored as **Higher \rightarrow Lower**.

270 Here, \mathcal{W}_q and \mathcal{W}_k are learnable projection matrices applied to \mathbf{O}_i and \mathbf{X}^{ref} , respectively. The resulting
 271 attention map $\mathbf{A}^i \in \mathbb{R}^{l \times Nh w}$ captures the relevance between the target pose and reference features.
 272 To obtain the final reference correlation scores, we compute the mean along the first dimension of
 273 \mathbf{A}^i using $\text{mean}(\cdot) : \mathbb{R}^{l \times Nh w} \rightarrow \mathbb{R}^{Nh w}$. In this context, l is the token number of \mathbf{O}_i , h and w denote
 274 the height and width of \mathbf{X}^{ref} , and d is the feature dimension of $\mathcal{W}_q \mathbf{O}_i$ and $\mathcal{W}_k \mathbf{X}^{\text{ref}}$. We further apply
 275 AvgPool to smooth the predicted correlation map and ReLU to suppress negative values.
 276

277 The correlation maps of PCFA are based on fine-grained semantic correlation between target bodies
 278 and DINO features of references. Unlike previous methods [26, 39] that depend on landmark
 279 similarity, our correlation map encodes richer outfit details, enabling more accurate reconstruction.

280 **Feature Selection.** The predicted correlation maps enable PCFA to selectively aggregate the most
 281 informative reference features for each target view. Specifically, we utilize ReferenceNet \mathcal{R} as the
 282 reference image encoder to extract multi-scale reference features $\mathbf{F} = \{\mathbf{F}_1, \mathbf{F}_2, \dots, \mathbf{F}_L\}$, where L
 283 is the number of layers. For each target pose \mathbf{P}_i and the reference feature $\mathbf{F}_k \in \mathbb{R}^{NS_k \times c}$ at layer k ,
 284 we first interpolate the corresponding correlation map $\mathbf{C}^i \in \mathbb{R}^{Nh w}$ to get $\hat{\mathbf{C}}^i = \text{Interp}_k(\mathbf{C}^i)$ that
 285 aligns with the spatial dimensions of \mathbf{F}_k . Here S_k denotes the spatial size of \mathbf{F}_k , and $\text{Interp}_k(\cdot) : \mathbb{R}^{Nh w} \rightarrow \mathbb{R}^{NS_k}$ denotes the interpolation operator.
 286

287 We then select the most relevant reference features $\hat{\mathbf{F}}_k^i$ for view \mathbf{P}_i based on $\hat{\mathbf{C}}^i$. Specifically, we
 288 employ the topk selection strategy to obtain the selected indices of \mathbf{F}_k :
 289

$$291 [k_1^i, k_2^i, \dots, k_{\gamma S_k}^i] = \text{sort}(\text{topk}(\hat{\mathbf{C}}^i)[: \gamma S_k]), \quad (3)$$

293 where $[k_1^i, k_2^i, \dots, k_{\gamma S_k}^i]$ are the indices of the selected features, $\text{topk}(\cdot)$ returns the top γS_k indices,
 294 and γ controls the proportion of features retained. To preserve spatial order, we apply $\text{sort}(\cdot)$.
 295

296 Using these indices, we extract the selected reference features $\hat{\mathbf{F}}_k^i \in \mathbb{R}^{\gamma S_k \times c}$:

$$298 \hat{\mathbf{F}}_k^i = \mathbf{F}_k[k_1^i, k_2^i, \dots, k_{\gamma S_k}^i] \cdot \hat{\mathbf{C}}_i[k_1^i, k_2^i, \dots, k_{\gamma S_k}^i]. \quad (4)$$

300 Given the aggregated reference features $\hat{\mathbf{F}} = \{\hat{\mathbf{F}}_k^1, \hat{\mathbf{F}}_k^2, \dots, \hat{\mathbf{F}}_k^M\}_{k=1}^L$, we synthesize the orthogonal
 301 multi-view images as $\mathbf{V} = \mathcal{D}^{\text{rgb}}(\hat{\mathbf{F}}, \mathcal{P}^{\text{rgb}}(\mathbf{P}))$, where \mathcal{D}^{rgb} is our multi-view image generation model
 302 and $\mathcal{P}^{\text{rgb}}(\cdot)$ is the pose guider that encodes the pose condition into \mathcal{D}^{rgb} .
 303

3.2 NORMAL MAP GENERATION AND MESH RECONSTRUCTION

307 For multi-view reconstruction (MVS) [51, 54, 91],
 308 we generate multi-view clothed normal maps \mathbf{N} from
 309 the generated images \mathbf{V} , conditioned on target poses
 310 \mathbf{P} , and reconstruct the mesh using both \mathbf{V} and \mathbf{N} .

311 **Normal Map Generation.** To ensure multi-view consistency and provide strong geometric cues for
 312 normal map generation, we follow [93] and incorporate
 313 SMPL-X normal renderings as additional conditions.
 314 As Fig. 5 shows, we also adopt MV-Adapter as the
 315 backbone of clothed normal generator $\mathcal{D}^{\text{normal}}$. We
 316 utilize the generated orthogonal RGB views \mathbf{V} as ref-
 317 erence inputs, and employ the pose guider $\mathcal{P}^{\text{normal}}(\cdot)$
 318 to incorporate multi-view pose conditions. The multi-view clothed normal maps are then generated
 319 via $\mathbf{N} = \mathcal{D}^{\text{normal}}(\mathbf{V}, \mathcal{P}^{\text{normal}}(\mathbf{P}))$.
 320

321 **Mesh Carving and Texture Baking.** Starting from the initial SMPLX mesh, we refine mesh details
 322 using the generated \mathbf{N} and project per-vertex colors from \mathbf{V} , following PSHuman [48]. To better
 323 preserve hand geometry, we replace the hand region with that from the initial mesh as in ECON [93],
 324 and then perform texture baking using the generated multi-view RGB images.

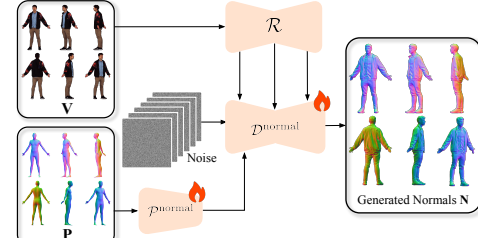


Figure 5: **Normal Map Generation Pipeline.** The main input difference with Fig. 3 is the generated multi-view orthogonal images \mathbf{V} , instead of unconstrained inputs \mathbf{I} .

	PuzzleIOI						4D-Dress						in-the-wild	
	PSNR↑	SSIM↑	LPIPS↓	Chamfer↓	P2S↓	Normal↓	PSNR↑	SSIM↑	LPIPS↓	Chamfer↓	P2S↓	Normal↓	CLIP-I↑	DINO↑
AvatarBooth	16.879	0.860	0.1544	6.635	6.697	0.0274	18.186	0.850	0.1718	6.846	6.978	0.0311	0.878	0.619
PuzzleAvatar	21.664	0.916	0.0639	3.204	3.165	0.0150	21.376	0.887	0.1081	1.956	2.045	0.0170	0.907	0.742
Ours (Image)	23.896	0.926	0.0545	-	-	-	25.848	0.920	0.0576	-	-	-	0.972	0.932
Ours (Mesh)	24.539	0.940	0.0474	2.724	2.605	0.0115	25.540	0.918	0.0654	1.140	1.119	0.0122	0.971	0.916

Table 1: Quantitative Comparison with Baselines. UP2You achieves the best texture fidelity, geometry accuracy, and perception similarity.

3.3 MULTI-REFERENCE SHAPE PREDICTOR

The initial SMPL-X mesh is critical to the entire UP2You pipeline, as it provides the pose condition \mathbf{P} for multi-view generation and serves as the basis for mesh reconstruction. SMPL-X mesh $\mathbf{T} \in \mathbb{R}^{10754 \times 3}$ are defined as $\mathbf{T}(\beta, \theta, \psi)$, where β, θ, ψ are shape, pose, and expression parameters respectively. While the target pose and expression of the SMPL-X template can be predefined (e.g., T-pose or A-pose with neutral expression), the body shape parameters must be estimated from unconstrained input images. Existing shape predictors [23, 48, 65] are typically designed for single-image scenarios and struggle to effectively leverage multiple unconstrained references.

To address this limitation, we introduce a multi-reference shape predictor, \mathcal{S} , as illustrated in Fig. 6. The prediction process is formulated as $\beta^{\text{pred}} = \mathcal{S}(\tau, \mathbf{X}^{\text{ref}})$, where β^{pred} denotes the predicted shape parameters, τ are learnable query tokens, and \mathbf{X}^{ref} are DINOv2 features extracted from the reference images. Our shape predictor \mathcal{S} employs a perceiver-style architecture [34, 46] that can use query tokens to effectively aggregate multi-view information. The prediction head is a lightweight transformer, similar to the camera head design in [87].

Overall, through the shape predictor, multi-view image & normal generator, and mesh carving & texture baking steps, UP2You generates textured 3D humans from unconstrained photo inputs. See the detailed flowchart in *Sup.Mat.*’s Appendix D.5.

4 EXPERIMENTS

4.1 SETTINGS

Dataset. We train our multi-view image generation, normal map generation, and shape prediction models on the THuman2.1 [99], Human4DiT [74], 2K2K [20], and CustomHumans [24] datasets. For evaluation, we use the PuzzleIOI [94] and 4D-Dress [88] datasets as test sets. To further validate our approach, we collect an in-the-wild (in-the-wild) dataset comprising 12 distinct identities. Details on dataset selection and processing procedures are provided in Appendix D.2.

Baselines. We comprehensively compare UP2You with 1) album-to-human reconstruction methods, including PuzzleAvatar [94] and AvatarBooth [102]. Since single-view reconstruction is a special case of the unconstrained setting, we also include the leading 2) single-view method, PSHuman [48], in our comparisons. To ensure fair evaluation and isolate the impact of pose estimation errors, we provide ground truth SMPL-X parameters for all baseline methods. 3) For shape prediction, we present the first approach to estimate SMPL-X shape parameters from multiple unconstrained inputs. We compare our shape predictor with two single-input methods: Semantify [17], which is specifically designed for shape prediction, and PromptHMR [89], a state-of-the-art human mesh recovery method. Unless stated otherwise, results on PuzzleIOI and 4D-Dress use 12 reference images. 4) For in-the-wild, we use all available references (8–12) for each identity. Additional model and training details are in *Sup.Mat.*’s Appendices D.1 and D.3.

Metrics. For PuzzleIOI and 4D-Dress (with textured 3D GT), we report geometric metrics (Chamfer, P2S, Normal map L2) and image quality metrics (PSNR, SSIM, LPIPS). For in-the-wild, we use perceptual similarity (CLIP-I, DINO) between generated and frontal reference. Shape prediction is assessed by vertex-to-vertex (V2V) distance on all datasets. More details in *Sup.Mat.*’s Appendix D.4.

4.2 COMPARISONS

Quantitative Results. The quantitative results in Tab. 1 show that UP2You consistently surpasses all baselines across both 2D and 3D evaluation metrics on the PuzzleIOI and 4D-Dress datasets.

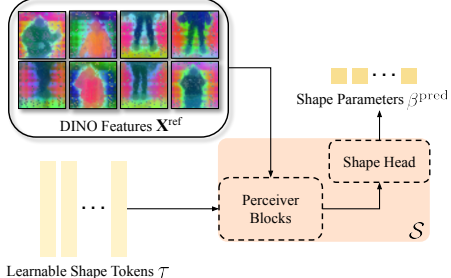


Figure 6: Multi-reference Shape Predictor.

Figure 8: Qualitative Comparisons on PuzzleIOI and 4D-Dress. See more 360-degree results in *Sup. Mat.*'s [video](#).

Importantly, UP2You also achieves strong perceptual quality scores on the in-the-wild dataset, demonstrating its robustness and effectiveness in real-world unconstrained scenarios.

For single-view reconstruction, Tab. 3 shows that UP2You outperforms PSHuman on all 2D and 3D metrics. This is expected, as single front-view input is a special case of the unconstrained multi-view scenario for which UP2You is designed. Training on the more challenging unconstrained task enables our model to generalize well and excel in the simpler constrained setting.

As shown in Tab. 2 and Fig. 7, our shape predictor outperforms single-view methods [17, 89], achieving more accurate and consistent results. Single-input baselines show high variance and instability, especially with partial input or failed detections. Leveraging multiple inputs, our method delivers more robust shape prediction, with performance further improving as more unconstrained references are used. **Furthermore, Table 2 also shows that the perceiver transformer architecture is better than simple MLPs for the shape predictor.**

Num of References	Semantify		PromptHMR		MLP	Ours
	Mean↓	Var↓	Mean↓	Var↓		
3	11.087	4.234	9.212	10.370	8.819	7.967
6	11.066	5.706	9.661	17.465	8.046	7.427
9	10.978	6.424	9.403	18.218	8.275	7.403
12	11.097	6.597	9.287	19.418	8.336	7.399

Table 2: V2V(↓) Comparisons of Shape Prediction Results.

Qualitative Results. The qualitative comparisons in Fig. 8 and Fig. 9 show that UP2You achieves high-fidelity, reference-faithful 3D reconstructions with strong realism and detail preservation. In contrast, baselines like AvatarBooth and PuzzleAvatar often fail to capture fine facial details and produce blurrier, less realistic results with poor subject-specific consistency. Figure 10 shows single-

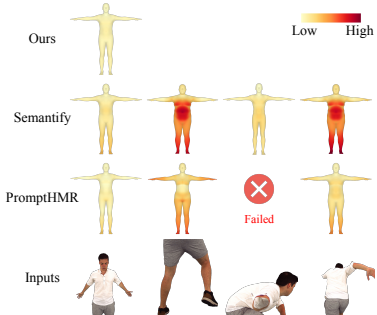


Figure 7: Shape Prediction Error Map.

	PSNR↑	SSIM↑	LPIPS↓	Chamfer↓	P2S↓	Normal↓
PSHuman	24.134	0.905	0.0895	2.759	2.926	0.0189
Ours Mesh	26.651	0.935	0.0527	0.927	0.949	0.0096

Table 3: Comparison of Single-Image based Reconstruction.

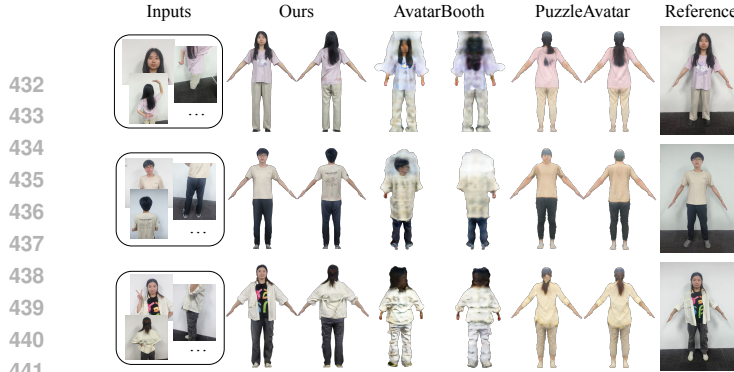


Figure 9: Qualitative Comparisons on in-the-wild Data.

view 3D human reconstruction comparisons. Our method generalizes well to single-view inputs, producing visually comparable results to PSHuman, but with more accurate limb reconstruction due to consistent multi-view guidance. More visual comparisons and results are in Appendices E.1 and G.

	Feature Aggregation					Image Encoder			PuzzleIOI			4D-Dress		
	Mean	Concat	Corr.	sum	topk	CLIP	DINOv2	Ref Net	PSNR↑	SSIM↑	LPIPS↓	PSNR↑	SSIM↑	LPIPS↓
Ours	✗	✗	✓	✗	✓	✗	✗	✓	23.896	0.926	0.0545	25.848	0.920	0.0576
A.	✓	✗	✗	✗	✗	✗	✗	✓	17.412	0.864	0.1227	19.614	0.876	0.1098
B.	✗	✓	✗	✗	✗	✗	✗	✓	20.545	0.893	0.0949	23.366	0.901	0.0791
C.	✗	✗	✓	✓	✗	✗	✗	✓	20.167	0.889	0.1002	23.412	0.904	0.0794
D.	✗	✗	✓	✗	✓	✓	✗	✗	20.152	0.891	0.0976	23.405	0.903	0.0801
E.	✗	✗	✓	✗	✓	✗	✓	✗	19.744	0.886	0.1415	23.393	0.904	0.0813

Table 4: Ablation Studies of our orthogonal view image generation model.

455

4.3 ABLATION STUDIES

Multi-View Image Generation. In Tab. 4, we analyze our multi-view image generation model on the PuzzleIOI and 4D-Dress datasets. For feature aggregation, we compare simple averaging (A), concatenation (B), and our proposed PCFA, which achieves the best results. We also test a weighted sum strategy (C) after correlation map prediction. For reference feature extraction, we evaluate CLIP (D), DINOv2 (E), and ReferenceNet. Quantitative and visual results (Appendix F.1) show our design outperforms all alternatives.

Correlation Maps. Our correlation map prediction module identifies and prioritizes key regions in reference images based on the target pose. As shown in Figure 11, visualizations for front- and back-view targets confirm that our maps effectively select the most relevant areas for view generation. This targeted focus improves generation quality and reduces GPU memory usage by retaining only the most informative features. More visual results are shown in Appendix E.2.

Number of References. In Tab. 5, quality improves as more unconstrained references are used. PCFA module efficiently selects informative features, keeping GPU memory usage low, unlike direct concatenation, which increases memory linearly.

Robustness to Inputs & Conditions. The generated human identity remains consistent across different target poses and reference combinations, with detailed discussions and results presented in *Sup. Mat.*'s Appendix F.2 and Appendix F.3. Notably, UP2You can effectively handle subjects with loose clothing and complex target poses, as demonstrated in Fig. 24 of Appendix F.2.

Image Encoder of PCFA. Given that DINOv2 has been demonstrated to effectively capture 2D-to-3D correspondences [58], we adopt it as the image encoder for our PCFA module. To further validate this design choice, we conduct additional experiments on the 4D-Dress dataset using alternative image encoders, including CLIP [68] and DINOv1 [8]. As presented in Tab. 6, DINOv2 consistently outperforms both alternatives on multi-view image generation quality.

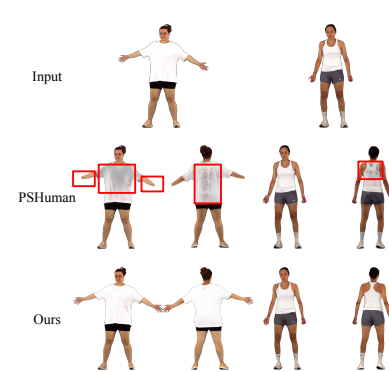


Figure 10: UP2You vs. PSHuman.



Figure 11: Predicted Correlation Maps.
See dynamic illustration of correlation maps in *Sup. Mat.*'s video.

	Ours				Concat			
	PSNR↑	SSIM↑	LPIPS↓	GPU↓	PSNR↑	SSIM↑	LPIPS↓	GPU↓
3 refs	24.159	0.912	0.0680	18.65	22.759	0.897	0.0894	18.02
6 refs	25.041	0.917	0.0623	19.40	23.267	0.901	0.0807	24.33
9 refs	25.646	0.918	0.0592	20.16	23.362	0.901	0.0796	30.89
12 refs	25.848	0.920	0.0576	20.88	23.366	0.901	0.0791	37.96

Table 5: Multi-View Generation with Different Number of References.

486
487
488
489
490
491
492
Figure 12: Generation Results on Highly Occluded Inputs.

Figure 13: Generation Results on Missing Part.

	PSNR↑	SSIM↑	LPIPS↓
DINOv2	25.848	0.920	0.0576
CLIP	23.876	0.904	0.0767
DINOv1	24.170	0.907	0.0745

	PSNR↑	SSIM↑	LPIPS↓	GPU↓
$\gamma = 1.0$	24.978	0.912	0.0665	18.64
$\gamma = 2.0$	25.848	0.920	0.0576	20.88
$\gamma = 3.0$	25.837	0.920	0.0569	23.12

493
494
495
496
Table 6: Comparison of Different Image Encoders for PCFA. Table 7: Comparison of Different Number of Selected Features.

497
498
499
500
501
502
Number of Selected Features. We set the default value of γ to 2.0 to control the number of reference
502 features selected in the `topk` selection. To determine the optimal configuration, we evaluate different
503 values of γ as shown in Table 7. The results demonstrate that $\gamma = 2.0$ achieves the best trade-off
504 between generation quality and GPU memory efficiency.

505
506
507
508
509
510
511
512
513
514
Unconstrained Inputs vs. Single Front View. Compared to single full-body front-view inputs, unconstrained photos are easier to collect and capture richer information about side and back views. Using the comprehensive information from unconstrained photos leads to better reconstruction results. Table 8 compares UP2You against standard single front-view based methods on 4D-Dress dataset, including ICON [92], ECON [93], PIFuHD [72], PSHuman [48], and Human3Diff [96]. Our method achieves the best performance in both rendering quality and 3D accuracy, particularly for back-view rendering results, demonstrating the value of unconstrained inputs.

	PSNR↑				SSIM↑		LPIPS↓		Chamfer↓	P2S↓	Normal↓
	Front	Back	Front	Back	Front	Back	Front	Back			
Ours*	25.257	25.488	0.906	0.909	0.0724	0.0733	1.140	1.119	0.0122		
PSHuman	25.384	23.382	0.898	0.885	0.0934	0.1121	2.756	2.926	0.0189		
Human3Diff	23.335	20720	0.883	0.872	0.1118	0.1248	4.275	4.322	0.0227		
ICON	-	-	-	-	-	-	4.352	4.331	0.0188		
ECON	-	-	-	-	-	-	3.780	3.642	0.0178		
PIFuHD	-	-	-	-	-	-	2.776	2.603	0.0154		

515
516
517
518
519
520
521
522
Table 8: Unconstrained Photos vs. Single Front View. * indicates our method uses unconstrained photos input, while other methods use single full-body front view input.

523
524
525
526
527
528
Generated Results in Extreme Situation. UP2You is robust to input variations and can effectively extract information from highly occluded photos. Figure 12 presents an example where one input image captures only the foot region, while other images lack this body part, demonstrating the capability of our method to handle inputs with high occlusion ratios. Figure 13 further examines scenarios where body parts are not fully visible across all images (e.g. the foot region). Due to diffusion hallucination, the generated results exhibit a somewhat reasonable structure; however, the texture is blended from other visible parts (more cases shown in *Sup.Mat.*'s Fig. 29). Therefore, inputs with complete body part coverage are more suitable for UP2You to achieve optimal results.

529
530
531
Animation. Since we adopt the A-Pose as the default target pose, the reconstructed mesh is naturally suited for animation. The textured mesh generated by UP2You can be easily animated using third-party tools such as Mixamo [6]. Moreover, the aligned SMPL-X parameters provided by UP2You enable animation based on skin weight transfer [1]. Finally, as UP2You can transform unconstrained inputs into different target pose configurations, animated rendering results can also be directly performed by itself, as demonstrated in *Sup.Mat.*'s Fig. 21.

5 CONCLUSION

532
533
534
535
536
537
538
539
UP2You acts as a “data rectifier,” converting unconstrained photos into orthogonal views suitable for MVS. It is efficient (1.5 minutes per person on one GPU), achieves SOTA quality, and well preserves identity and clothing style across diverse input forms and pose conditions. It also enables free 3D virtual try-on (Fig. 14, more in *Sup.Mat.*'s Fig. 30). Limitations and future work are discussed in *Sup.Mat.*'s Appendix H.



Figure 14: 3D Virtual Try-On.

540 REFERENCES
541

- 542 [1] Rinat Abdashitov, Kim Raichstat, Jared Monsen, and David Hill. Robust skin weights transfer
543 via weight inpainting. In *SIGGRAPH Asia 2023 Technical Communications*, 2023. 10, 26
- 544 [2] Yuval Alaluf, Elad Richardson, Gal Metzer, and Daniel Cohen-Or. A neural space-time
545 representation for text-to-image personalization. *Transactions on Graphics (TOG)*, 2023. 4, 19
- 546 [3] Badour AlBahar, Shunsuke Saito, Hung-Yu Tseng, Changil Kim, Johannes Kopf, and Jia-Bin
547 Huang. Single-image 3d human digitization with shape-guided diffusion. In *International
548 Conference on Computer Graphics and Interactive Techniques in Asia (SIGGRAPH Asia)*,
549 2023. 3
- 550 [4] Omri Avrahami, Kfir Aberman, Ohad Fried, Daniel Cohen-Or, and Dani Lischinski. Break-
551 a-scene: Extracting multiple concepts from a single image. In *International Conference on
552 Computer Graphics and Interactive Techniques in Asia (SIGGRAPH Asia)*, 2023. 4, 19
- 553 [5] Jinze Bai, Shuai Bai, Shusheng Yang, Shijie Wang, Sinan Tan, Peng Wang, Junyang Lin, Chang
554 Zhou, and Jingren Zhou. Qwen-vl: A frontier large vision-language model with versatile
555 abilities. *arXiv preprint arXiv:2308.12966*, 2023. 19
- 556 [6] Sue Blackman. Rigging with mixamo. In *Unity for Absolute Beginners*. Springer, 2014. 10, 26
- 557 [7] Zeyu Cai, Duotun Wang, Yixun Liang, Zhijing Shao, Ying-Cong Chen, Xiaohang Zhan, and
558 Zeyu Wang. Dreammapping: High-fidelity text-to-3d generation via variational distribution
559 mapping. In *Pacific Conference on Computer Graphics and Applications (PG)*, 2024. 4
- 560 [8] Mathilde Caron, Hugo Touvron, Ishan Misra, Hervé Jégou, Julien Mairal, Piotr Bojanowski,
561 and Armand Joulin. Emerging properties in self-supervised vision transformers. In *International
562 Conference on Computer Vision (ICCV)*, 2021. 9
- 563 [9] Bowei Chen, Brian Curless, Ira Kemelmacher-Shlizerman, and Steven M Seitz. Total selfie:
564 generating full-body selfies. In *Proc. IEEE Conf. on Computer Vision and Pattern Recognition
565 (CVPR)*, 2024. 4, 19
- 566 [10] Bardienus Pieter Duisterhof, Lojze Zust, Philippe Weinzaepfel, Vincent Leroy, Yohann Cabon,
567 and Jerome Revaud. Mast3r-sfm: a fully-integrated solution for unconstrained structure-from-
568 motion. In *International Conference on 3D Vision (3DV)*, 2025. 4
- 569 [11] Facebook. DINOv2-Large. [https://huggingface.co/facebook/
570 dinov2-large](https://huggingface.co/facebook/dinov2-large), 2023. 20
- 571 [12] Yao Feng, Vasileios Choutas, Timo Bolkart, Dimitrios Tzionas, and Michael J Black. Collabora-
572 tive regression of expressive bodies using moderation. In *International Conference on 3D
573 Vision (3DV)*, 2021. 3
- 574 [13] Yarden Frenkel, Yael Vinker, Ariel Shamir, and Daniel Cohen-Or. Implicit style-content
575 separation using b-lora. In *European Conference on Computer Vision (ECCV)*, 2024. 4, 19
- 576 [14] Rinon Gal, Yuval Alaluf, Yuval Atzmon, Or Patashnik, Amit H Bermano, Gal Chechik, and
577 Daniel Cohen-Or. An image is worth one word: Personalizing text-to-image generation using
578 textual inversion. *arXiv preprint arXiv:2208.01618*, 2022. 4, 19
- 579 [15] Xiangjun Gao, Xiaoyu Li, Chaopeng Zhang, Qi Zhang, Yanpei Cao, Ying Shan, and Long
580 Quan. Context-human: Free-view rendering of human from a single image with texture-
581 consistent synthesis. In *Proc. IEEE Conf. on Computer Vision and Pattern Recognition
582 (CVPR)*, 2024. 3
- 583 [16] Daniel Garibi, Shahar Yadin, Roni Paiss, Omer Tov, Shiran Zada, Ariel Ephrat, Tomer Michaeli,
584 Inbar Mosseri, and Tali Dekel. Tokenverse: Versatile multi-concept personalization in token
585 modulation space. *Transactions on Graphics (TOG)*, 2025. 4, 19
- 586 [17] Omer Gralnik, Guy Gafni, and Ariel Shamir. Semantify: Simplifying the control of 3d
587 morphable models using clip. In *International Conference on Computer Vision (ICCV)*, 2023.
588 7, 8

- 594 [18] Chen Guo, Tianjian Jiang, Xu Chen, Jie Song, and Otmar Hilliges. Vid2avatar: 3d avatar
 595 reconstruction from videos in the wild via self-supervised scene decomposition. In *Proc. IEEE*
 596 *Conf. on Computer Vision and Pattern Recognition (CVPR)*, 2023. 1, 3
 597
- 598 [19] Chen Guo, Junxuan Li, Yash Kant, Yaser Sheikh, Shunsuke Saito, and Chen Cao. Vid2avatar-
 599 pro: Authentic avatar from videos in the wild via universal prior. In *Proc. IEEE Conf. on*
 600 *Computer Vision and Pattern Recognition (CVPR)*, 2025. 3
- 601 [20] Sang-Hun Han, Min-Gyu Park, Ju Hong Yoon, Ju-Mi Kang, Young-Jae Park, and Hae-Gon
 602 Jeon. High-fidelity 3d human digitization from single 2k resolution images. In *Proc. IEEE*
 603 *Conf. on Computer Vision and Pattern Recognition (CVPR)*, 2023. 7, 20
- 604 [21] Xinyang Han, Zelin Gao, Angjoo Kanazawa, Shubham Goel, and Yossi Gal. The
 605 more you see in 2d the more you perceive in 3d. In *Proc. IEEE Conf. on Computer Vision and*
 606 *Pattern Recognition (CVPR)*, 2024. 3
- 607 [22] Kaiming He, Xiangyu Zhang, Shaoqing Ren, and Jian Sun. Deep residual learning for image
 608 recognition. In *Proc. IEEE Conf. on Computer Vision and Pattern Recognition (CVPR)*, 2016.
 609 20
- 610 [23] Xu He, Zhiyong Wu, Xiaoyu Li, Di Kang, Chaopeng Zhang, Jiangnan Ye, Liyang Chen,
 611 Xiangjun Gao, Han Zhang, and Haolin Zhuang. Magicman: Generative novel view synthesis
 612 of humans with 3d-aware diffusion and iterative refinement. In *AAAI Conference on Artificial*
 613 *Intelligence*, 2025. 1, 2, 3, 7
- 614 [24] Hsuan-I Ho, Lixin Xue, Jie Song, and Otmar Hilliges. Learning locally editable virtual humans.
 615 In *Proc. IEEE Conf. on Computer Vision and Pattern Recognition (CVPR)*, 2023. 7, 20
- 616 [25] Jonathan Ho, Ajay Jain, and Pieter Abbeel. Denoising diffusion probabilistic models. In
 617 *Conference on Neural Information Processing Systems (NeurIPS)*, 2020. 3, 19
- 618 [26] Fa-Ting Hong, Zhan Xu, Haiyang Liu, Qinjie Lin, Luchuan Song, Zhixin Shu, Yang Zhou,
 619 Duygu Ceylan, and Dan Xu. Free-viewpoint human animation with pose-correlated reference
 620 selection. In *Proc. IEEE Conf. on Computer Vision and Pattern Recognition (CVPR)*, 2025. 5,
 621 6
- 622 [27] Li Hu, Xin Gao, Peng Zhang, Ke Sun, Bang Zhang, and Liefeng Bo. Animate anyone:
 623 Consistent and controllable image-to-video synthesis for character animation. In *Proc. IEEE*
 624 *Conf. on Computer Vision and Pattern Recognition (CVPR)*, 2024. 2, 4, 19
- 625 [28] Liangxiao Hu, Hongwen Zhang, Yuxiang Zhang, Boyao Zhou, Boning Liu, Shengping Zhang,
 626 and Liqiang Nie. Gaussianavatar: Towards realistic human avatar modeling from a single
 627 video via animatable 3d gaussians. In *Proc. IEEE Conf. on Computer Vision and Pattern*
 628 *Recognition (CVPR)*, 2024. 1, 3
- 629 [29] Han Huang, Liliang Chen, and Xihao Wang. Unconfuse: avatar reconstruction from uncon-
 630 strained images. In *European Conference on Computer Vision (ECCV)*, 2022. 3
- 631 [30] Xin Huang, Ruizhi Shao, Qi Zhang, Hongwen Zhang, Ying Feng, Yebin Liu, and Qing
 632 Wang. HumanNorm: Learning normal diffusion model for high-quality and realistic 3d human
 633 generation. In *Proc. IEEE Conf. on Computer Vision and Pattern Recognition (CVPR)*, 2024.
 634 3
- 635 [31] Yangyi Huang, Hongwei Yi, Yuliang Xiu, Tingting Liao, Jiaxiang Tang, Deng Cai, and
 636 Justus Thies. Tech: Text-guided reconstruction of lifelike clothed humans. In *International*
 637 *Conference on 3D Vision (3DV)*, 2024. 3
- 638 [32] Zehuan Huang, Yuan-Chen Guo, Haoran Wang, Ran Yi, Lizhuang Ma, Yan-Pei Cao, and
 639 Lu Sheng. Mv-adapter: Multi-view consistent image generation made easy. In *International*
 640 *Conference on Computer Vision (ICCV)*, 2025. 2, 4, 19, 20
- 641 [33] Zeng Huang, Yuanlu Xu, Christoph Lassner, Hao Li, and Tony Tung. Arch: Animatable
 642 reconstruction of clothed humans. In *Proc. IEEE Conf. on Computer Vision and Pattern*
 643 *Recognition (CVPR)*, 2020. 3

- 648 [34] Andrew Jaegle, Felix Gimeno, Andy Brock, Oriol Vinyals, Andrew Zisserman, and Joao
649 Carreira. Perceiver: General perception with iterative attention. In *International Conference
650 on Machine Learning (ICML)*, 2021. 2, 7
- 651
652 [35] Tianjian Jiang, Xu Chen, Jie Song, and Otmar Hilliges. Instantavatar: Learning avatars
653 from monocular video in 60 seconds. In *Proc. IEEE Conf. on Computer Vision and Pattern
654 Recognition (CVPR)*, 2023. 1, 3
- 655 [36] Yudong Jin, Sida Peng, Xuan Wang, Tao Xie, Zhen Xu, Yifan Yang, Yujun Shen, Hujun Bao,
656 and Xiaowei Zhou. Diffuman4d: 4d consistent human view synthesis from sparse-view videos
657 with spatio-temporal diffusion models. *arXiv preprint arXiv:2507.13344*, 2025. 3
- 658
659 [37] Oren Katzir, Or Patashnik, Daniel Cohen-Or, and Dani Lischinski. Noise-free score distillation.
660 In *International Conference on Learning Representations (ICLR)*, 2024. 4
- 661 [38] Byungjun Kim, Patrick Kwon, Kwangho Lee, Myunggi Lee, Sookwan Han, Daesik Kim, and
662 Hanbyul Joo. Chupa: Carving 3d clothed humans from skinned shape priors using 2d diffusion
663 probabilistic models. In *International Conference on Computer Vision (ICCV)*, 2023. 3
- 664
665 [39] Xianghao Kong, Qiaosong Qi, Yuanbin Wang, Anyi Rao, Biaolong Chen, Aixi Zhang, Si Liu,
666 and Hao Jiang. Profashion: Prototype-guided fashion video generation with multiple reference
667 images. *arXiv preprint arXiv:2505.06537*, 2025. 5, 6
- 668 [40] Nupur Kumari, Bingliang Zhang, Richard Zhang, Eli Shechtman, and Jun-Yan Zhu. Multi-
669 concept customization of text-to-image diffusion. In *Proc. IEEE Conf. on Computer Vision
670 and Pattern Recognition (CVPR)*, 2023. 4, 19
- 671
672 [41] Nupur Kumari, Xi Yin, Jun-Yan Zhu, Ishan Misra, and Samaneh Azadi. Generating multi-
673 image synthetic data for text-to-image customization. *arXiv preprint arXiv:2502.01720*, 2025.
674 4, 19
- 675 [42] Black Forest Labs. Flux. <https://github.com/black-forest-labs/flux>, 2024.
676 3, 19
- 677
678 [43] Boqian Li, Haiwen Feng, Zeyu Cai, Michael J Black, and Yuliang Xiu. Etch: Generalizing
679 body fitting to clothed humans via equivariant tightness. In *International Conference on
680 Computer Vision (ICCV)*, 2025. 3
- 681 [44] Boqian Li, Xuan Li, Ying Jiang, Tianyi Xie, Feng Gao, Huamin Wang, Yin Yang, and
682 Chenfanfu Jiang. Garmentdreamer: 3dgs guided garment synthesis with diverse geometry and
683 texture details. In *International Conference on 3D Vision (3DV)*, 2025. 3
- 684
685 [45] Jiefeng Li, Chao Xu, Zhicun Chen, Siyuan Bian, Lixin Yang, and Cewu Lu. Hybrik: A hybrid
686 analytical-neural inverse kinematics solution for 3d human pose and shape estimation. In *Proc.
687 IEEE Conf. on Computer Vision and Pattern Recognition (CVPR)*, 2021. 3
- 688
689 [46] Junnan Li, Dongxu Li, Silvio Savarese, and Steven Hoi. Blip-2: Bootstrapping language-
690 image pre-training with frozen image encoders and large language models. In *International
691 Conference on Machine Learning (ICML)*, 2023. 2, 7
- 692
693 [47] Peng Li, Yuan Liu, Xiaoxiao Long, Feihu Zhang, Cheng Lin, Mengfei Li, Xingqun Qi,
694 Shanghang Zhang, Wei Xue, Wenhan Luo, et al. Era3d: High-resolution multiview diffusion
695 using efficient row-wise attention. *Conference on Neural Information Processing Systems
696 (NeurIPS)*, 2024. 19
- 697
698 [48] Peng Li, Wangguandong Zheng, Yuan Liu, Tao Yu, Yangguang Li, Xingqun Qi, Xiaowei
699 Chi, Siyu Xia, Yan-Pei Cao, Wei Xue, et al. Pshuman: Photorealistic single-image 3d human
700 reconstruction using cross-scale multiview diffusion and explicit remeshing. In *Proc. IEEE
701 Conf. on Computer Vision and Pattern Recognition (CVPR)*, 2025. 1, 2, 3, 6, 7, 10, 19
- 702
703 [49] Yihui Li, Chengxin Lv, Hongyu Yang, and Di Huang. Micro-macro wavelet-based gaussian
704 splatting for 3d reconstruction from unconstrained images. In *AAAI Conference on Artificial
705 Intelligence*, 2025. 4

- 702 [50] Tingting Liao, Hongwei Yi, Yuliang Xiu, Jiaxiang Tang, Yangyi Huang, Justus Thies, and
 703 Michael J Black. Tada! text to animatable digital avatars. In *International Conference on 3D*
 704 *Vision (3DV)*, 2024. 3
- 705 [51] Tingting Liao, Yujian Zheng, Yuliang Xiu, Adilbek Karmanov, Liwen Hu, Leyang Jin, and Hao
 706 Li. SOAP: Style-omniscient animatable portraits. In *International Conference on Computer*
 707 *Graphics and Interactive Techniques (SIGGRAPH)*, 2025. 6
- 708 [52] Lixiang Lin, Songyou Peng, Qijun Gan, and Jianke Zhu. Fasthuman: Reconstructing high-
 709 quality clothed human in minutes. In *International Conference on 3D Vision (3DV)*, 2024.
 710 3
- 711 [53] Xian Liu, Xiaohang Zhan, Jiaxiang Tang, Ying Shan, Gang Zeng, Dahua Lin, Xihui Liu, and
 712 Ziwei Liu. Humangaussian: Text-driven 3d human generation with gaussian splatting. In *Proc.*
 713 *IEEE Conf. on Computer Vision and Pattern Recognition (CVPR)*, 2024. 3
- 714 [54] Xiaoxiao Long, Yuan-Chen Guo, Cheng Lin, Yuan Liu, Zhiyang Dou, Lingjie Liu, Yuexin
 715 Ma, Song-Hai Zhang, Marc Habermann, Christian Theobalt, et al. Wonder3d: Single image
 716 to 3d using cross-domain diffusion. In *Proc. IEEE Conf. on Computer Vision and Pattern*
 717 *Recognition (CVPR)*, 2024. 6
- 718 [55] Jia Lu, Taoran Yi, Jiemin Fang, Chen Yang, Chuiyun Wu, Wei Shen, Wenyu Liu, Qi Tian,
 719 and Xinggang Wang. Snap-snap: Taking two images to reconstruct 3d human gaussians in
 720 milliseconds. *arXiv preprint arXiv:2508.14892*, 2025. 1, 3
- 721 [56] Ben Mildenhall, Pratul P Srinivasan, Matthew Tancik, Jonathan T Barron, Ravi Ramamoorthi,
 722 and Ren Ng. Nerf: Representing scenes as neural radiance fields for view synthesis. In
 723 *European Conference on Computer Vision (ECCV)*, 2020. 4
- 724 [57] Maxime Oquab, Timothée Darivet, Théo Moutakanni, Huy Vo, Marc Szafraniec, Vasil Khalidov,
 725 Pierre Fernandez, Daniel Haziza, Francisco Massa, Alaaeldin El-Nouby, et al. Dinov2:
 726 Learning robust visual features without supervision. *Transactions on Machine Learning*
 727 *Research Journal (TMLR)*, 2024. 5
- 728 [58] Evin Pinar Örnek, Yann Labb  , Bugra Tekin, Lingni Ma, Cem Keskin, Christian Forster,
 729 and Tomas Hodan. Foundpose: Unseen object pose estimation with foundation features. In
 730 *European Conference on Computer Vision (ECCV)*, 2024. 9
- 731 [59] Zhuoyang Pan, Angjoo Kanazawa, and Hang Gao. SOAR: Self-occluded avatar recovery from
 732 a single video in the wild. *arXiv preprint arXiv:2410.23800*, 2024. 3
- 733 [60] Hao-Yang Peng, Jia-Peng Zhang, Meng-Hao Guo, Yan-Pei Cao, and Shi-Min Hu. Chartergen:
 734 Efficient 3d character generation from single images with multi-view pose canonicalization.
 735 *Transactions on Graphics (TOG)*, 2024. 2
- 736 [61] Sida Peng, Chen Geng, Yuanqing Zhang, Yinghao Xu, Qianqian Wang, Qing Shuai, Xiaowei
 737 Zhou, and Hujun Bao. Implicit neural representations with structured latent codes for human
 738 body modeling. *Transactions on Pattern Analysis and Machine Intelligence (TPAMI)*, 2023. 3
- 739 [62] Ben Poole, Ajay Jain, Jonathan T Barron, and Ben Mildenhall. Dreamfusion: Text-to-3d using
 740 2d diffusion. In *International Conference on Learning Representations (ICLR)*, 2023. 2, 4
- 741 [63] Guocheng Qian, Kuan-Chieh Wang, Or Patashnik, Negin Heravi, Daniil Ostashev, Sergey
 742 Tulyakov, Daniel Cohen-Or, and Kfir Aberman. Omni-id: Holistic identity representation
 743 designed for generative tasks. In *Proc. IEEE Conf. on Computer Vision and Pattern Recognition*
 744 *(CVPR)*, 2025. 4, 19
- 745 [64] Shenhan Qian, Tobias Kirschstein, Liam Schoneveld, Davide Davoli, Simon Giebenhain, and
 746 Matthias Nie  ner. Gaussianavatars: Photorealistic head avatars with rigged 3d gaussians. In
 747 *Proc. IEEE Conf. on Computer Vision and Pattern Recognition (CVPR)*, 2024. 1

- 756 [65] Lingteng Qiu, Xiaodong Gu, Peihao Li, Qi Zuo, Weichao Shen, Junfei Zhang, Kejie Qiu,
 757 Weihao Yuan, Guanying Chen, Zilong Dong, et al. Lhm: Large animatable human reconstruc-
 758 tion model from a single image in seconds. In *International Conference on Computer Vision*
 759 (*ICCV*), 2025. 1, 3, 7
- 760 [66] Lingteng Qiu, Peihao Li, Qi Zuo, Xiaodong Gu, Yuan Dong, Weihao Yuan, Siyu Zhu, Xi-
 761 aoguang Han, Guanying Chen, and Zilong Dong. Pf-lhm: 3d animatable avatar reconstruction
 762 from pose-free articulated human images. *arXiv preprint arXiv:2506.13766*, 2025. 3
- 764 [67] Lingteng Qiu, Shenhao Zhu, Qi Zuo, Xiaodong Gu, Yuan Dong, Junfei Zhang, Chao Xu,
 765 Zhe Li, Weihao Yuan, Liefeng Bo, et al. Anigs: Animatable gaussian avatar from a single
 766 image with inconsistent gaussian reconstruction. In *Proc. IEEE Conf. on Computer Vision and*
 767 *Pattern Recognition (CVPR)*, 2025. 3
- 768 [68] Alec Radford, Jong Wook Kim, Chris Hallacy, Aditya Ramesh, Gabriel Goh, Sandhini Agarwal,
 769 Girish Sastry, Amanda Askell, Pamela Mishkin, Jack Clark, et al. Learning transferable visual
 770 models from natural language supervision. In *International Conference on Machine Learning*
 771 (*ICML*), 2021. 9
- 773 [69] Robin Rombach, Andreas Blattmann, Dominik Lorenz, Patrick Esser, and Björn Ommer. High-
 774 resolution image synthesis with latent diffusion models. In *Proc. IEEE Conf. on Computer*
 775 *Vision and Pattern Recognition (CVPR)*, 2022. 3, 19
- 776 [70] Nataniel Ruiz, Yuanzhen Li, Varun Jampani, Yael Pritch, Michael Rubinstein, and Kfir Aber-
 777 man. Dreambooth: Fine tuning text-to-image diffusion models for subject-driven generation.
 778 In *Proc. IEEE Conf. on Computer Vision and Pattern Recognition (CVPR)*, 2023. 2, 3, 4, 19
- 780 [71] Shunsuke Saito, Zeng Huang, Ryota Natsume, Shigeo Morishima, Angjoo Kanazawa, and
 781 Hao Li. Pifu: Pixel-aligned implicit function for high-resolution clothed human digitization.
 782 In *International Conference on Computer Vision (ICCV)*, 2019. 3
- 784 [72] Shunsuke Saito, Tomas Simon, Jason Saragih, and Hanbyul Joo. Pifuhd: Multi-level pixel-
 785 aligned implicit function for high-resolution 3d human digitization. In *Proc. IEEE Conf. on*
 786 *Computer Vision and Pattern Recognition (CVPR)*, 2020. 3, 10
- 787 [73] Viraj Shah, Nataniel Ruiz, Forrester Cole, Erika Lu, Svetlana Lazebnik, Yuanzhen Li, and
 788 Varun Jampani. Ziplora: Any subject in any style by effectively merging loras. In *European*
 789 *Conference on Computer Vision (ECCV)*, 2024. 4, 19
- 791 [74] Ruizhi Shao, Youxin Pang, Zerong Zheng, Jingxiang Sun, and Yebin Liu. 360-degree human
 792 video generation with 4d diffusion transformer. *Transactions on Graphics (TOG)*, 2024. 7, 20
- 793 [75] Fei Shen and Jinhui Tang. Imagpose: A unified conditional framework for pose-guided person
 794 generation. *Conference on Neural Information Processing Systems (NeurIPS)*, 2024. 4, 19
- 796 [76] Tianchang Shen, Jun Gao, Kangxue Yin, Ming-Yu Liu, and Sanja Fidler. Deep marching
 797 tetrahedra: a hybrid representation for high-resolution 3d shape synthesis. *Conference on*
 798 *Neural Information Processing Systems (NeurIPS)*, 2021. 4
- 800 [77] Ruoxi Shi, Hansheng Chen, Zhuoyang Zhang, Minghua Liu, Chao Xu, Xinyue Wei, Linghao
 801 Chen, Chong Zeng, and Hao Su. Zero123++: a single image to consistent multi-view diffusion
 802 base model. *arXiv preprint arXiv:2310.15110*, 2023. 19
- 803 [78] Yichun Shi, Peng Wang, Jianglong Ye, Long Mai, Kejie Li, and Xiao Yang. Mvdream: Multi-
 804 view diffusion for 3d generation. In *International Conference on Learning Representations*
 805 (*ICLR*), 2024. 19
- 807 [79] Yukai Shi, Jianan Wang, Boshi Tang, Xianbiao Qi, Tianyu Yang, Yukun Huang, Shilong Liu,
 808 Lei Zhang, Heung-Yeung Shum, et al. Toss: High-quality text-guided novel view synthesis
 809 from a single image. In *International Conference on Learning Representations (ICLR)*, 2024.
 19

- 810 [80] Noah Snavely, Steven M Seitz, and Richard Szeliski. Photo tourism: Exploring photo collections in 3d. In *International Conference on Computer Graphics and Interactive Techniques (SIGGRAPH)*, 2006. 4
- 811
- 812
- 813
- 814 [81] Jiaming Song, Chenlin Meng, and Stefano Ermon. Denoising diffusion implicit models. In *International Conference on Learning Representations (ICLR)*, 2021. 3, 19
- 815
- 816 [82] Stabilityai. Stable-Diffusion-2-1-Base. <https://huggingface.co/stabilityai/stable-diffusion-2-1-base>, 2023. 20
- 817
- 818
- 819 [83] Jiapeng Tang, Davide Davoli, Tobias Kirschstein, Liam Schoneveld, and Matthias Niessner. Gaf: Gaussian avatar reconstruction from monocular videos via multi-view diffusion. In *Proc. IEEE Conf. on Computer Vision and Pattern Recognition (CVPR)*, 2025. 3
- 820
- 821
- 822 [84] Luming Tang, Nataniel Ruiz, Qinghao Chu, Yuanzhen Li, Aleksander Holynski, David E Jacobs, Bharath Hariharan, Yael Pritch, Neal Wadhwa, Kfir Aberman, et al. Realfill: Reference-driven generation for authentic image completion. *Transactions on Graphics (TOG)*, 2024. 2, 4, 19
- 823
- 824
- 825
- 826 [85] Andrey Voynov, Qinghao Chu, Daniel Cohen-Or, and Kfir Aberman. p+: Extended textual conditioning in text-to-image generation. *arXiv preprint arXiv:2303.09522*, 2023. 4, 19
- 827
- 828
- 829 [86] Duotun Wang, Hengyu Meng, Zeyu Cai, Zhijing Shao, Qianxi Liu, Lin Wang, Mingming Fan, Xiaohang Zhan, and Zeyu Wang. Headevolver: Text to head avatars via expressive and attribute-preserving mesh deformation. In *International Conference on 3D Vision (3DV)*, 2025. 3
- 830
- 831
- 832
- 833 [87] Jianyuan Wang, Minghao Chen, Nikita Karaev, Andrea Vedaldi, Christian Rupprecht, and David Novotny. Vggt: Visual geometry grounded transformer. In *Proc. IEEE Conf. on Computer Vision and Pattern Recognition (CVPR)*, 2025. 4, 7
- 834
- 835
- 836
- 837 [88] Wenbo Wang, Hsuan-I Ho, Chen Guo, Boxiang Rong, Artur Grigorev, Jie Song, Juan Jose Zarate, and Otmar Hilliges. 4d-dress: A 4d dataset of real-world human clothing with semantic annotations. In *Proc. IEEE Conf. on Computer Vision and Pattern Recognition (CVPR)*, 2024. 7, 20
- 838
- 839
- 840
- 841 [89] Yufu Wang, Yu Sun, Priyanka Patel, Kostas Daniilidis, Michael J Black, and Muhammed Kocabas. Prompthmr: Promptable human mesh recovery. In *Proc. IEEE Conf. on Computer Vision and Pattern Recognition (CVPR)*, 2025. 3, 7, 8
- 842
- 843
- 844
- 845 [90] Chung-Yi Weng, Brian Curless, Pratul P Srinivasan, Jonathan T Barron, and Ira Kemelmacher-Shlizerman. Humannerf: Free-viewpoint rendering of moving people from monocular video. In *Proc. IEEE Conf. on Computer Vision and Pattern Recognition (CVPR)*, 2022. 3
- 846
- 847
- 848 [91] Kailu Wu, Fangfu Liu, Zhihan Cai, Runjie Yan, Hanyang Wang, Yating Hu, Yueqi Duan, and Kaisheng Ma. Unique3d: High-quality and efficient 3d mesh generation from a single image. *Conference on Neural Information Processing Systems (NeurIPS)*, 2024. 6
- 849
- 850
- 851
- 852 [92] Yuliang Xiu, Jinlong Yang, Dimitrios Tzionas, and Michael J Black. Icon: Implicit clothed humans obtained from normals. In *Proc. IEEE Conf. on Computer Vision and Pattern Recognition (CVPR)*, 2022. 1, 3, 10
- 853
- 854
- 855 [93] Yuliang Xiu, Jinlong Yang, Xu Cao, Dimitrios Tzionas, and Michael J Black. Econ: Explicit clothed humans optimized via normal integration. In *Proc. IEEE Conf. on Computer Vision and Pattern Recognition (CVPR)*, 2023. 1, 3, 6, 10
- 856
- 857
- 858 [94] Yuliang Xiu, Yufei Ye, Zhen Liu, Dimitrios Tzionas, and Michael J Black. Puzzleavatar: Assembling 3d avatars from personal albums. *Transactions on Graphics (TOG)*, 2024. 2, 3, 4, 7, 20
- 859
- 860
- 861
- 862 [95] Yifang Xu, Benxiang Zhai, Yunzhuo Sun, Ming Li, Yang Li, and Sidan Du. Hifi-portrait: zero-shot identity-preserved portrait generation with high-fidelity multi-face fusion. In *Proc. IEEE Conf. on Computer Vision and Pattern Recognition (CVPR)*, 2025. 4, 19
- 863

- 864 [96] Yuxuan Xue, Xianghui Xie, Riccardo Marin, and Gerard Pons-Moll. Human-3diffusion:
 865 Realistic avatar creation via explicit 3d consistent diffusion models. *Conference on Neural*
 866 *Information Processing Systems (NeurIPS)*, 2024. 10
 867
- 868 [97] Xihe Yang, Xingyu Chen, Daiheng Gao, Shaohui Wang, Xiaoguang Han, and Baoyuan Wang.
 869 Have-fun: Human avatar reconstruction from few-shot unconstrained images. In *Proc. IEEE*
 870 *Conf. on Computer Vision and Pattern Recognition (CVPR)*, 2024. 3
 871
- 872 [98] Wanqi Yin, Zhongang Cai, Ruiyi Wang, Ailing Zeng, Chen Wei, Qingping Sun, Haiyi Mei,
 873 Yanjun Wang, Hui En Pang, Mingyuan Zhang, et al. Smplest-x: Ultimate scaling for expressive
 874 human pose and shape estimation. *arXiv preprint arXiv:2501.09782*, 2025. 3
 875
- 876 [99] Tao Yu, Zerong Zheng, Kaiwen Guo, Pengpeng Liu, Qionghai Dai, and Yebin Liu. Function4d:
 877 Real-time human volumetric capture from very sparse consumer rgbd sensors. In *Proc. IEEE*
 878 *Conf. on Computer Vision and Pattern Recognition (CVPR)*, 2021. 7, 20
 879
- 880 [100] Xin Yu, Yuan-Chen Guo, Yangguang Li, Ding Liang, Song-Hai Zhang, and Xiaojuan Qi. Text-
 881 to-3d with classifier score distillation. In *International Conference on Learning Representations*
 882 (*ICLR*), 2024. 4
 883
- 884 [101] Zhiyuan Yu, Zhe Li, Hujun Bao, Can Yang, and Xiaowei Zhou. Humanram: Feed-forward
 885 human reconstruction and animation model using transformers. In *International Conference*
 886 *on Computer Graphics and Interactive Techniques (SIGGRAPH)*, 2025. 1, 3
 887
- 888 [102] Yifei Zeng, Yuanxun Lu, Xinya Ji, Yao Yao, Hao Zhu, and Xun Cao. Avatarbooth: High-
 889 quality and customizable 3d human avatar generation. *arXiv preprint arXiv:2306.09864*, 2023.
 890 2, 3, 4, 7
 891
- 892 [103] Yu Zeng, Vishal M Patel, Haochen Wang, Xun Huang, Ting-Chun Wang, Ming-Yu Liu, and
 893 Yogesh Balaji. Jedi: Joint-image diffusion models for finetuning-free personalized text-to-
 894 image generation. In *Proc. IEEE Conf. on Computer Vision and Pattern Recognition (CVPR)*,
 895 2024. 4, 19
 896
- 897 [104] Hongwen Zhang, Yating Tian, Xinchi Zhou, Wanli Ouyang, Yebin Liu, Limin Wang, and
 898 Zhenan Sun. Pymaf: 3d human pose and shape regression with pyramidal mesh alignment
 899 feedback loop. In *International Conference on Computer Vision (ICCV)*, 2021. 3
 900
- 901 [105] Jingbo Zhang, Xiaoyu Li, Qi Zhang, Yanpei Cao, Ying Shan, and Jing Liao. Humanref:
 902 Single image to 3d human generation via reference-guided diffusion. In *Proc. IEEE Conf. on*
 903 *Computer Vision and Pattern Recognition (CVPR)*, 2024. 3
 904
- 905 [106] Peng Zheng, Dehong Gao, Deng-Ping Fan, Li Liu, Jorma Laaksonen, Wanli Ouyang, and
 906 Nicu Sebe. Bilateral reference for high-resolution dichotomous image segmentation. *CAAI*
 907 *Artificial Intelligence Research*, 2024. 21
 908
- 909 [107] Zerong Zheng, Tao Yu, Yebin Liu, and Qionghai Dai. Pamir: Parametric model-conditioned im-
 910 plicit representation for image-based human reconstruction. *Transactions on Pattern Analysis*
 911 *and Machine Intelligence (TPAMI)*, 2021. 3
 912
- 913 [108] Xiangyu Zhu, Tingting Liao, Xiaomei Zhang, Jiangjing Lyu, Zhiwen Chen, Yunfeng Wang,
 914 Kan Guo, Qiong Cao, Stan Z Li, and Zhen Lei. MVP-Human Dataset for 3-D clothed human
 915 avatar reconstruction from multiple frames. *IEEE Transactions on Biometrics, Behavior, and*
 916 *Identity Science*, 2023. 3
 917
- 918 [109] Zhuofan Zong, Dongzhi Jiang, Bingqi Ma, Guanglu Song, Hao Shao, Dazhong Shen, Yu Liu,
 919 and Hongsheng Li. Easyref: Omni-generalized group image reference for diffusion models
 920 via multimodal llm. In *International Conference on Machine Learning (ICML)*, 2024. 4, 19
 921

918
919
920
921
922
923

Appendix

Table of Contents

924	A Use of Large Language Models	19
925		
926	B Related Work	19
927	B.1 Subject-driven and ID-consistent Image Generation	19
928		
929	C Priliminary	19
930		
931	D Implementation Details	20
932	D.1 Model Structure	20
933	D.2 Dataset	20
934	D.3 Training Details	20
935	D.4 Evaluation Metrics	20
936	D.5 Inference Process	21
937		
938	E Additional Visual Comparisons	22
939	E.1 Qualitative Comparisons	22
940	E.2 Correlation Maps	25
941	E.3 Animation Results	26
942	F Additional Ablation Studies	27
943	F.1 Visual Results of Different Orthogonal Images Generation Designs	27
944	F.2 Robustness of Target Pose Condition.	28
945	F.3 Analysis of Shape Predictor.	30
946	F.4 Visual Results with Different Number of Inputs	31
947		
948	G More Generation Results of UP2You	32
949		
950	H Limitations and Future Works	36
951		
952		
953		
954		
955		
956		
957		
958		
959		
960		
961		
962		
963		
964		
965		
966		
967		
968		
969		
970		
971		

972 **A USE OF LARGE LANGUAGE MODELS**
973974 We used a large language model to assist with copy editing—grammar checking, wording suggestions,
975 and minor style and clarity improvements—after the scientific content, methodology, analyses, and
976 conclusions had been written by the authors.
977978 **B RELATED WORK**
979980 **B.1 SUBJECT-DRIVEN AND ID-CONSISTENT IMAGE GENERATION**
981982 With the advent of powerful generative models [25, 42, 69, 81], subject-driven image generation has
983 made remarkable progress in recent years. Various approaches have been proposed to generate images
984 of specific subjects, such as optimizing specialized tokens to encode subject concepts [2, 14, 85],
985 learning personalized modulation vectors for each concept [16], or fine-tuning pre-trained diffusion
986 models [4, 13, 40, 70, 73] using a handful of reference images. Additionally, methods like JeDi [103]
987 and SynCD [41] utilize global self-attention mechanisms to effectively fuse information from multiple
988 images of a target subject, while EasyRef [109] leverages Vision-Language Models (VLMs) [5].
989990 For human-centric generation, several methods have been developed to handle identity preservation.
991 For instance, Omni-ID [63], IMAGPose [75], and HiFi-Portrait [95] utilize specialized image encoders
992 to process multiple reference images for ID-preserving image synthesis. However, extending these
993 techniques to the full body is non-trivial, as the human body’s highly articulated structure and non-
994 rigid deformations introduce significant challenges for feature fusion. To tackle this, approaches like
995 Total Selfie [9], and RealFill [84] employ few-shot personalization via fine-tuning [70] to capture
996 consistent identities, including both facial features and overall appearance. Nevertheless, these
997 methods are tailored for 2D image generation and lack the mechanisms needed to ensure cross-view
998 consistency or the precise latent feature aggregation required for high-fidelity 3D reconstruction.
9991000 **C PRILIMINARY**1001 We review the fundamentals of multi-view diffusion models [47, 77–79], with a particular focus on
1002 MV-Adapter [32], which serves as the foundation for the multi-view generation of UP2You.
10031004 **Multi-View Diffusion Models.** Multi-view diffusion models extend single-view generation by
1005 introducing multi-view attention mechanisms, enabling the synthesis of images that are consistent
1006 across different viewpoints. Several works [78, 79] generalize the self-attention mechanism of
1007 standard diffusion models to operate over all pixels from multiple views. Specifically, given f^{in} as the
1008 input to the attention block, multi-view self-attention concatenates features from M views, allowing
1009 the model to capture global dependencies. However, this approach incurs significant computational
1010 overhead due to the need to process all pixels across all views. To mitigate this, row-wise self-
1011 attention [47, 48] leverages geometric correspondences between orthogonal views. For example,
1012 Era3D [47] restricts attention to the current view and corresponding rows from other views, which is
1013 well-suited for orthogonal multi-view generation and substantially reduces computational cost.
10141015 Building on row-wise self-attention, MV-Adapter [32] introduces an image-to-multiview (I2MV)
1016 generator with a parallel attention architecture. The original self-attention block is modified as:
1017

1018
$$f^{\text{self}} = \text{SelfAttn}(f^{\text{in}}) + \text{MVAttn}(f^{\text{in}}) + \text{RefAttn}(f^{\text{in}}, \mathbf{F}) + f^{\text{in}}, \quad (5)$$

1019 Here, MVAttn represents the row-wise self-attention mechanism, while RefAttn is a cross-
1020 attention module that integrates the reference image feature \mathbf{F} into f^{in} . The feature \mathbf{F} is extracted from
1021 the input image \mathbf{I} using the reference network \mathcal{R} [27]: $\mathbf{F} = \mathcal{R}(\mathbf{I})$. The I2MV generation process in
1022 MV-Adapter is formulated as $\mathbf{V} = \mathcal{D}(\mathbf{F}, \mathcal{P}(\mathbf{P}))$, where $\mathbf{V} = \{\mathbf{V}_1, \mathbf{V}_2, \dots, \mathbf{V}_M\}$ denotes the set of
1023 generated multi-view images, \mathcal{D} represents the multi-view diffusion model, $\mathbf{P} = \{\mathbf{P}_1, \mathbf{P}_2, \dots, \mathbf{P}_M\}$
1024 specifies the target viewpoint conditions, and \mathcal{P} is the condition encoder that fuses viewpoint con-
1025 ditions into \mathcal{D} . In MV-Adapter, only MVAttn , RefAttn , and \mathcal{P} are trained for I2MV generation.
1026 Each \mathbf{P} is encoded as a camera ray representation, referred to as a “raymap”. Typically, $M = 6$ orthog-
1027 onal views are generated, corresponding to the target view angles $\{0^\circ, 45^\circ, 90^\circ, 135^\circ, 180^\circ, 270^\circ\}$.
1028

1026 Given the efficient plug-and-play adapter training mechanism of MV-Adapter, combined with the
 1027 robust feature extraction capabilities of ReferenceNet for processing unconstrained photographs, we
 1028 adopt MV-Adapter as our multi-view diffusion model architecture. Furthermore, considering our
 1029 focus on human-centric tasks, we utilize SMPL-X normal rendering as the viewpoint condition \mathbf{P} .
 1030

1031 D IMPLEMENTATION DETAILS

1032 D.1 MODEL STRUCTURE

1035 We adopt the framework architecture of MV-Adapter [32] with the
 1036 stable-diffusion-2-1-base version [82] as the foundation for both multi-view im-
 1037 age and normal generation. The number of selected reference features γ is set to 2.0 during both
 1038 training and inference phases. We employ the DINOv2-Large [11] variant of the DINOv2 encoder
 1039 \mathcal{E}^{ref} . For the pose image encoder \mathcal{E}^{ref} , we implement a lightweight ResNet [22] architecture. The
 1040 learnable shape tokens $\tau \in \mathbb{R}^{10 \times 1024}$ are configured to align with the dimensions of \mathcal{E}^{ref} , and the
 1041 perceiver blocks in \mathcal{S} comprise 6 layers of cross-attention.

1042 D.2 DATASET

1043 We train our multi-view image generation, normal map generation, and shape prediction models
 1044 using the THuman2.1 [99], Human4DiT [74], 2K2K [20], and CustomHumans [24] datasets. Since
 1045 our task requires handling scenarios where individuals with the same identity appear in different
 1046 poses, we manually filter the data and group samples by identity. The final training dataset com-
 1047 prises 6,921 scans spanning 2,091 distinct identities. For each scan, we render 6 orthogonal views
 1048 ($\{0^\circ, 45^\circ, 90^\circ, 135^\circ, 180^\circ, 270^\circ\}$) of both images and normal maps, along with the corresponding
 1049 SMPL-X normal rendering. Additionally, we render 8 views of each scan using randomly selected
 1050 perspective cameras to provide “unconstrained photos”. During orthogonal image generation training,
 1051 for each case, we randomly select 3 to 8 reference images from other cases sharing the same identity.
 1052

1053 For evaluation, we select 40 identities from PuzzleIOI [94] and additionally choose “A-pose” con-
 1054 figurations from all 68 identities in 4D-Dress [88], while utilizing the remaining poses as reference
 1055 views. To ensure that SMPL-X camera normal rendering accurately represents viewpoint information,
 1056 we rotate all scans so that the front view corresponds to zero azimuth. Beyond synthetic data, we
 1057 also collect an in-the-wild dataset comprising 12 identities for further evaluation, ensuring robust
 1058 evaluation in diverse scenarios.

1059 D.3 TRAINING DETAILS

1060 We train the image and normal generation models end-to-end using denoising losses $\mathcal{L}_d^{\text{rgb}}$ and $\mathcal{L}_d^{\text{normal}}$,
 1061 respectively. During training, $\mathcal{L}_d^{\text{rgb}}$ jointly optimizes the components $\mathcal{E}^{\text{pose}}$, \mathcal{T} , \mathcal{W}_q , \mathcal{W}_k , AvgPool,
 1062 \mathcal{P}^{rgb} , and \mathcal{D}^{rgb} . In normal maps generation training, $\mathcal{L}_d^{\text{normal}}$ optimizes $\mathcal{P}^{\text{normal}}$ and $\mathcal{D}^{\text{normal}}$. For shape
 1063 prediction, we employ the loss function $\mathcal{L}_v = |\mathbf{T}(\beta^{\text{pred}}) - \mathbf{T}(\beta^{\text{gt}})|$ to compute the vertex-wise
 1064 distance between SMPL-X meshes generated from the predicted shape parameters β^{pred} and the
 1065 ground-truth shape parameters β^{gt} .

1066 The complete training process for the image and normal generation models requires approximately 3
 1067 and 2 days, respectively, on 8 NVIDIA 5880 GPUs. We employ a batch size of 1 per GPU under
 1068 bfloat16 mixed precision and train for 50,000 iterations. All pose, input, and output image resolutions
 1069 are consistently set to 768×768 . The reference images for both image and normal generation are
 1070 also configured at 768×768 resolution, while the target orthogonal view angles follow the same
 1071 configuration as MV-Adapter. The shape prediction model undergoes training for 100,000 iterations
 1072 on 8 NVIDIA 5880 GPUs with a batch size of 8 per GPU, requiring approximately 10 hours. We
 1073 apply a constant learning rate of 5×10^{-5} with warm-up for training all models.

1074 D.4 EVALUATION METRICS

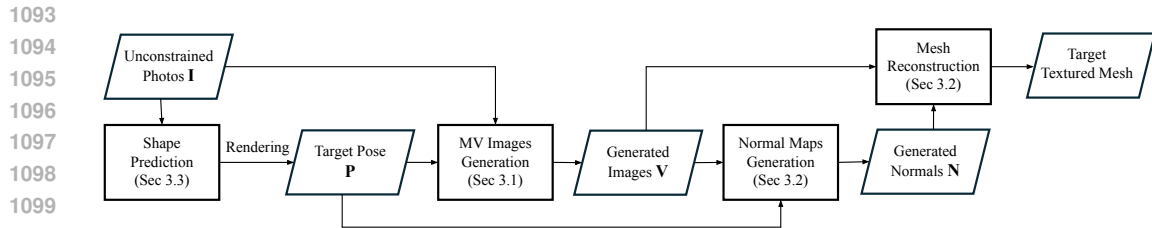
1075 We employ three complementary metrics to assess geometric accuracy: (1) **Chamfer distance**
 1076 (bidirectional point-to-surface distance in cm), which measures overall geometric similarity; (2) **P2S**

1080 **distance** (unidirectional point-to-surface distance in cm), which captures reconstruction completeness;
 1081 and (3) **L2 error for Normal maps** rendered from four canonical views ($\{0^\circ, 90^\circ, 180^\circ, 270^\circ\}$),
 1082 which evaluates fine-grained surface detail preservation.

1083 We render multi-view color images from the same four canonical viewpoints and evaluate appearance
 1084 fidelity using three established image quality metrics: **PSNR** (Peak Signal-to-Noise Ratio) for
 1085 pixel-level accuracy, **SSIM** (Structural Similarity) for structural consistency, and **LPIPS** (Learned
 1086 Perceptual Image Patch Similarity) for perceptual similarity.

1087 For the in-the-wild dataset, which lacks 3D ground truth, we assess reconstruction quality using
 1088 perceptual similarity metrics **CLIP-I** and **DINO** computed between the generated front view and the
 1089 captured reference front view image with A-pose.

1090 We further evaluate shape prediction accuracy by computing vertex-to-vertex (V2V) distances between
 1091 predicted and ground truth SMPL-X meshes under canonical T-pose (zero pose and expression).



1100 Figure 15: **Inference Process of UP2You.** Given only unconstrained photos \mathbf{I} as inputs, UP2You can generate a high-quality textured mesh.

1103 D.5 INference PROCESS

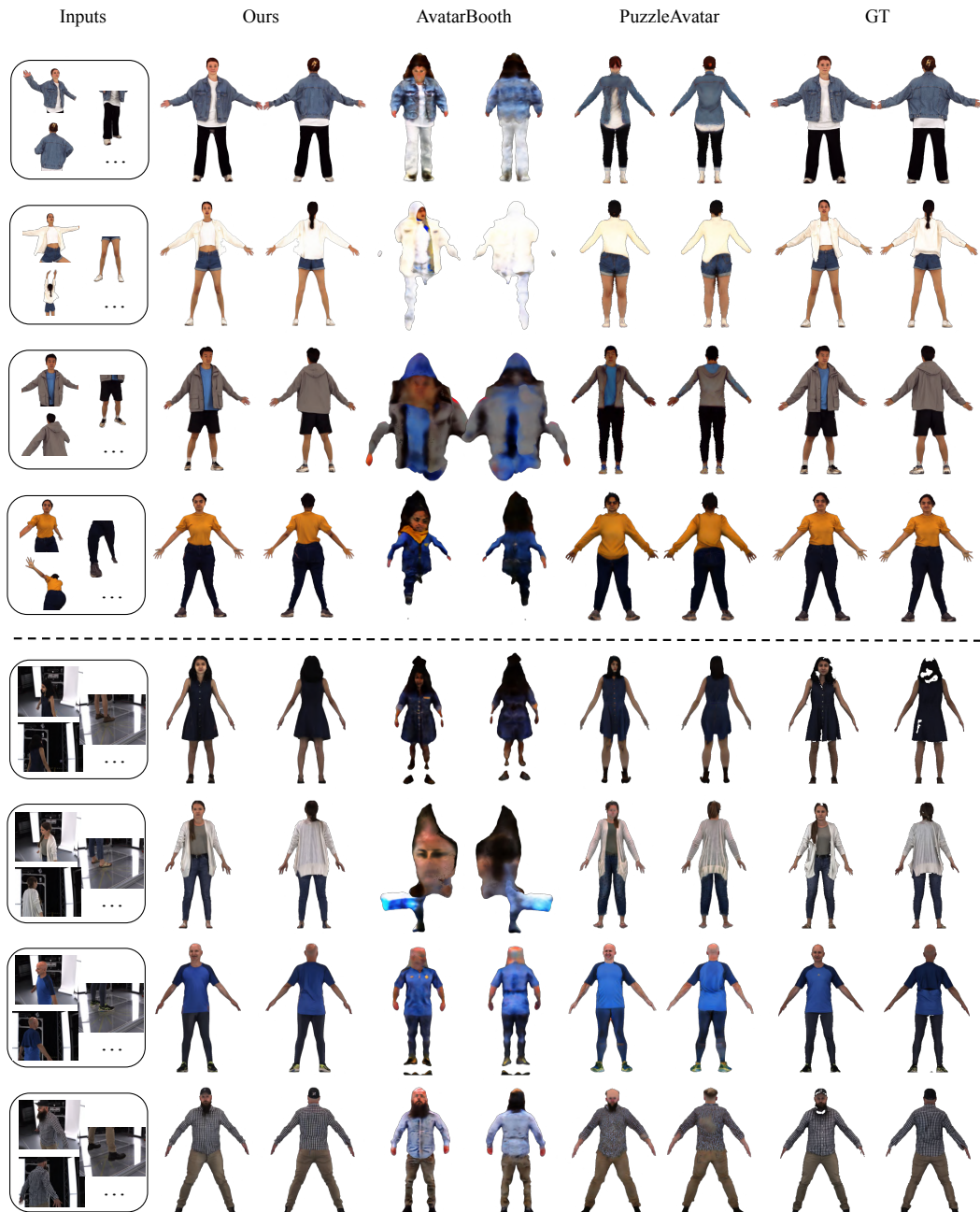
1104 The inference process of UP2You for unconstrained photo inputs \mathbf{I} is illustrated in Fig. 15, which
 1105 mainly consists of four steps as follows:

- 1106 (1) Use \mathcal{S} to estimate SMPL-X shape parameters β^{pred} from \mathbf{I} , and initialize the SMPL-X mesh with
 β^{pred} and a predefined pose (e.g., A-pose with zero expression) to obtain the pose condition \mathbf{P} .
- 1107 (2) Generate multi-view images \mathbf{V} using \mathcal{D}^{rgb} , conditioned on \mathbf{I} and \mathbf{P} .
- 1108 (3) Generate multi-view normal maps \mathbf{N} using $\mathcal{D}^{\text{normal}}$, conditioned on \mathbf{V} and \mathbf{P} .
- 1109 (4) Reconstruct the textured mesh using the initialized SMPL-X mesh, \mathbf{V} , and \mathbf{N} .

1110 For data pre- and post-processing, we employ [106] to remove backgrounds from input unconstrained
 1111 photos. Additionally, the reference masks are resized and adapted to the correlation maps \mathbf{C} to
 1112 enhance the model’s focus on foreground regions.

1113 **Inference Time.** The complete pipeline requires approximately 1.5 minutes to generate a textured
 1114 mesh from a single unconstrained input. Specifically, the shape prediction step takes about 1 second,
 1115 multi-view image generation requires approximately 15 seconds, normal map generation takes
 1116 about 15 seconds, and mesh reconstruction, along with other processing steps (e.g., foreground
 1117 segmentation, data postprocessing, and file saving), takes nearly 1 minute.

1118
 1119
 1120
 1121
 1122
 1123
 1124
 1125
 1126
 1127
 1128
 1129
 1130
 1131
 1132
 1133

1134 E ADDITIONAL VISUAL COMPARISONS
11351136 E.1 QUALITATIVE COMPARISONS
11371138 We present additional qualitative comparison results in Figs. 16 to 19, including mesh reconstruction,
1139 front-view 3D human reconstruction, and shape prediction comparisons. Please zoom in for details.
11401182 Figure 16: More Qualitative Comparisons on 4D-Dress and PuzzleIOI datasets.
1183
1184
1185
1186
1187

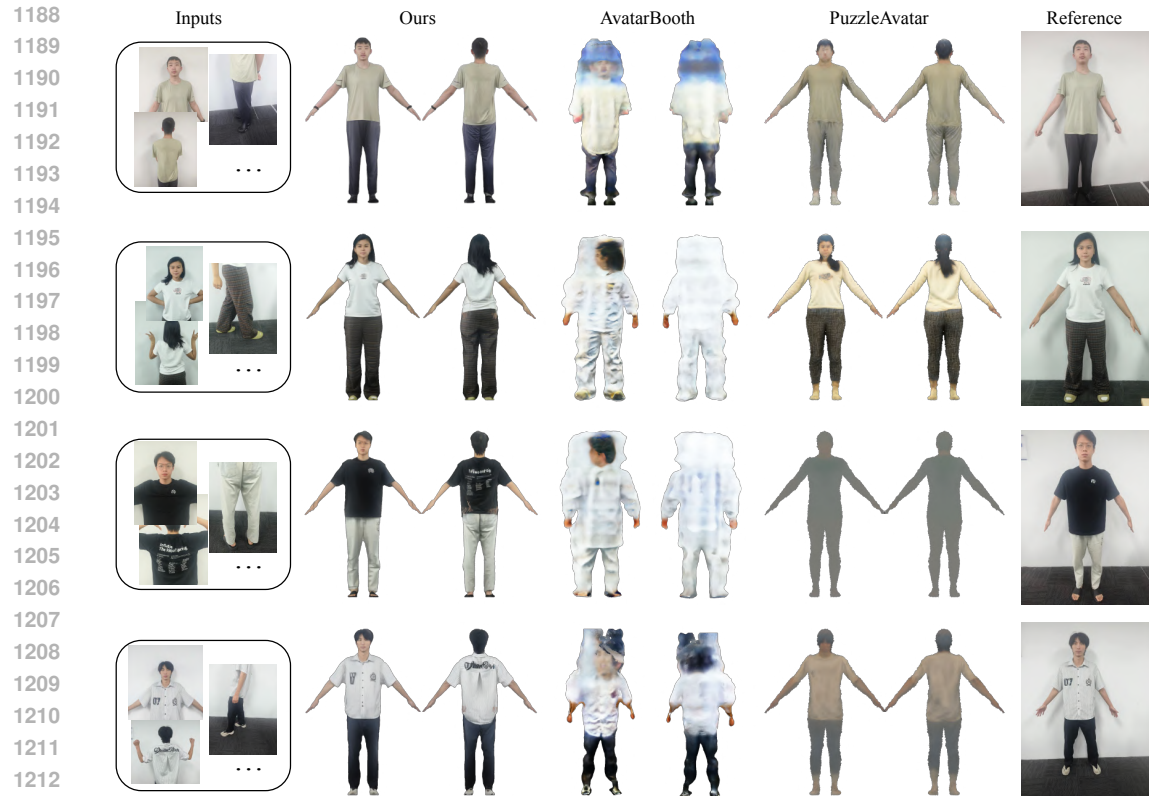


Figure 17: **More Qualitative Comparisons on in-the-wild dataset.**

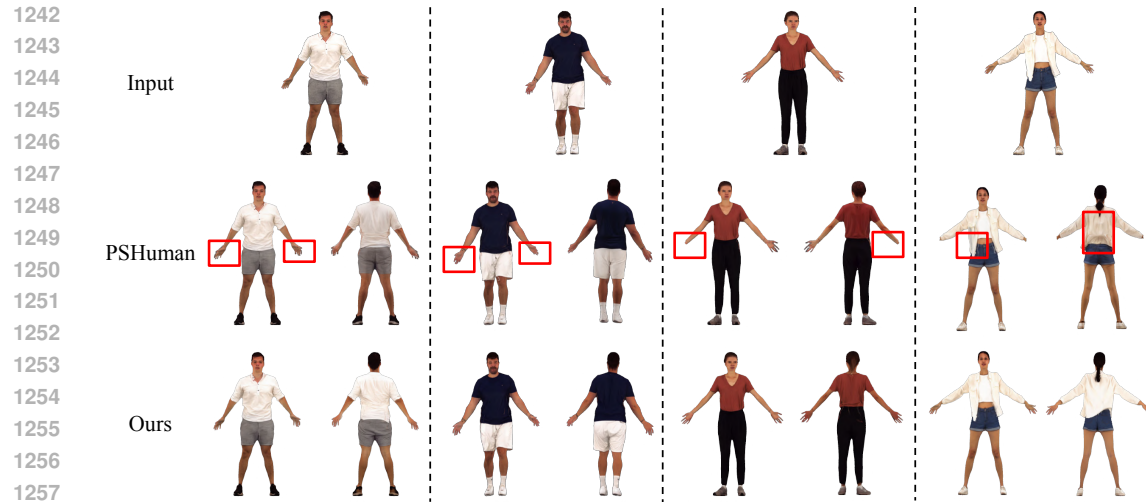


Figure 18: More Qualitative Comparisons of Single Image 3D Human Reconstruction with PSHuman.

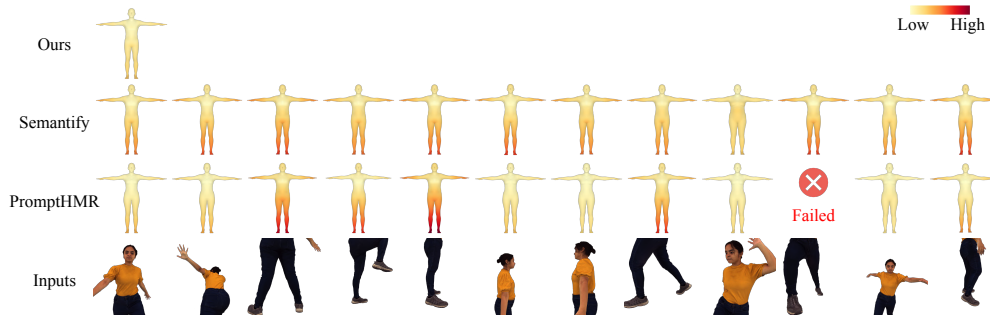


Figure 19: Error Maps of Shape Prediction.

1296
1297

E.2 CORRELATION MAPS

1298
1299
1300
1301

Pose-dependent correlation maps generation is an important module of UP2You, as the first part of the proposed PCFA, it predicts the most relevant regions of input unconstrained photos for the conditioned pose. With the latter feature selection strategy, PCFA can focus on informative features for viewpoint generation. In Fig. 20, we provide more results of the generated correlation maps.

1302



1303

1304

1305

1306

1307

1308

1309

1310

1311

1312

1313

1314

1315

1316

1317

1318

1319

1320

1321

1322

1323

1324

1325

1326

Figure 20: Visualize Results of Correlation Maps. Given the input reference images and target pose for multi-view image generation, the predicted correlation maps can effectively identify and discriminate correlated regions within the reference inputs. For example, when generating images in the front-view, reference regions that correspond to front-facing views exhibit higher correlation values, demonstrating the model’s ability to selectively attend to relevant spatial information.

1327

1328

1329

1330

1331

1332

1333

1334

1335

1336

1337

1338

1339

1340

1341

1342

1343

1344

1345

1346

1347

1348

1349

1350
1351

E.3 ANIMATION RESULTS

1352
1353
1354
1355
1356
1357

We present an animation sample generated by UP2You using the same reference with different target poses, as shown in Fig. 21. Notably, UP2You maintains identity consistency well across different target poses. However, since this approach just reconstructs a textured mesh independently for each frame, temporal consistency of the rendered images and mesh topology is not guaranteed. For production-quality animated sequences, we recommend using professional animation methods and tools [1, 6] for textured mesh animation.

1358

1359
1360
1361
1362
1363
1364
1365
1366
1367
1368
1369
1370
1371
1372
1373
1374
1375
1376
1377
1378
1379
1380
1381
1382
1383
1384
1385
1386
1387
1388
1389
1390
1391
1392
1393

Figure 21: Animation Results of Textured Mesh Generated by UP2You.

1394
1395
1396
1397
1398
1399
1400
1401
1402
1403

F ADDITIONAL ABLATION STUDIES

F.1 VISUAL RESULTS OF DIFFERENT ORTHOGONAL IMAGES GENERATION DESIGNS

Here, we present the generated visual results in Fig. 22 for different design choices in the multi-view image generation model. As indicated earlier, approach A directly concatenates all reference features for viewpoint generation, which may provide irrelevant features during generation and lead to poor results. Approach B averages all reference features as global guidance. This method is time-efficient but loses important color features and generates suboptimal results. Approach C uses a weighted sum strategy to aggregate reference features after computing the correlation map, which loses details in some regions since regions with high correlation values may overlap. Approaches D and E utilize CLIP and DINOv2 features, respectively, rather than ReferenceNet as in our method. CLIP features have low resolution and are difficult to preserve details such as facial and clothing textures, while DINOv2 is texture-insensitive and thus difficult to restore reference textures accurately.

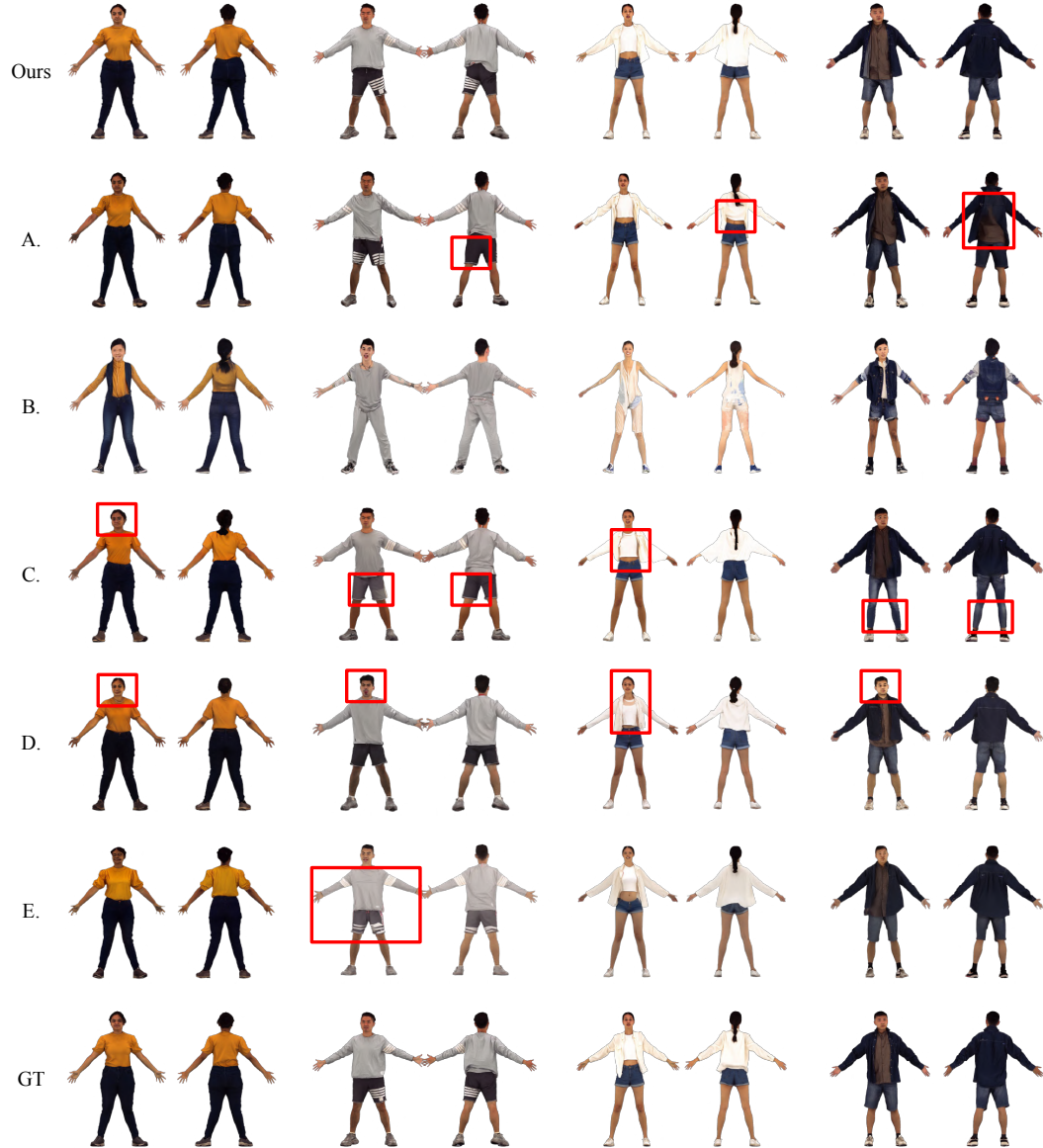


Figure 22: Visual Comparisons of Different Multi-View Image Generation Designs.

1458
1459

F.2 ROBUSTNESS OF TARGET POSE CONDITION.

1460
1461
1462
1463
1464
1465
1466
1467
1468
1469
1470

While previous experiments highlight the strong generation ability of UP2You, most target poses are in the “A-pose” configuration. Since 4D-Dress provides ground-truth multi-view images of persons with different poses, we further test robustness by randomly selecting three diverse target poses per identity from the 4D-Dress dataset and evaluating our multi-view image generation performance. As shown in Tab. 9, UP2You maintains high-quality results across varied target poses using the same unconstrained photo inputs. Figure 23 further demonstrates the visual results, where identity is consistently preserved across different poses. **In addition, Figure 24 shows the generation results on subjects with loose clothing and complex target poses, further validating the generation capability and robustness of UP2You.**

1471

1496
1497

Figure 23: **Robustness of target pose conditions.** Our method can generate high-quality multi-view images under different pose conditions with the same reference inputs, demonstrating that identity information is effectively disentangled from pose conditions in our approach.

1498
1499
1500
1501
1502
1503
1504
1505
1506
1507
1508
1509
1510
1511

	PSNR↑	SSIM↑	LPIPS↓
Pose A	24.983	0.911	0.0664
Pose B	24.400	0.902	0.0744
Pose C	24.519	0.904	0.0715

Table 9: **ID Consistency.** UP2You achieves high-quality multi-view image generation results in 4D-Dress dataset in three different pose condition.

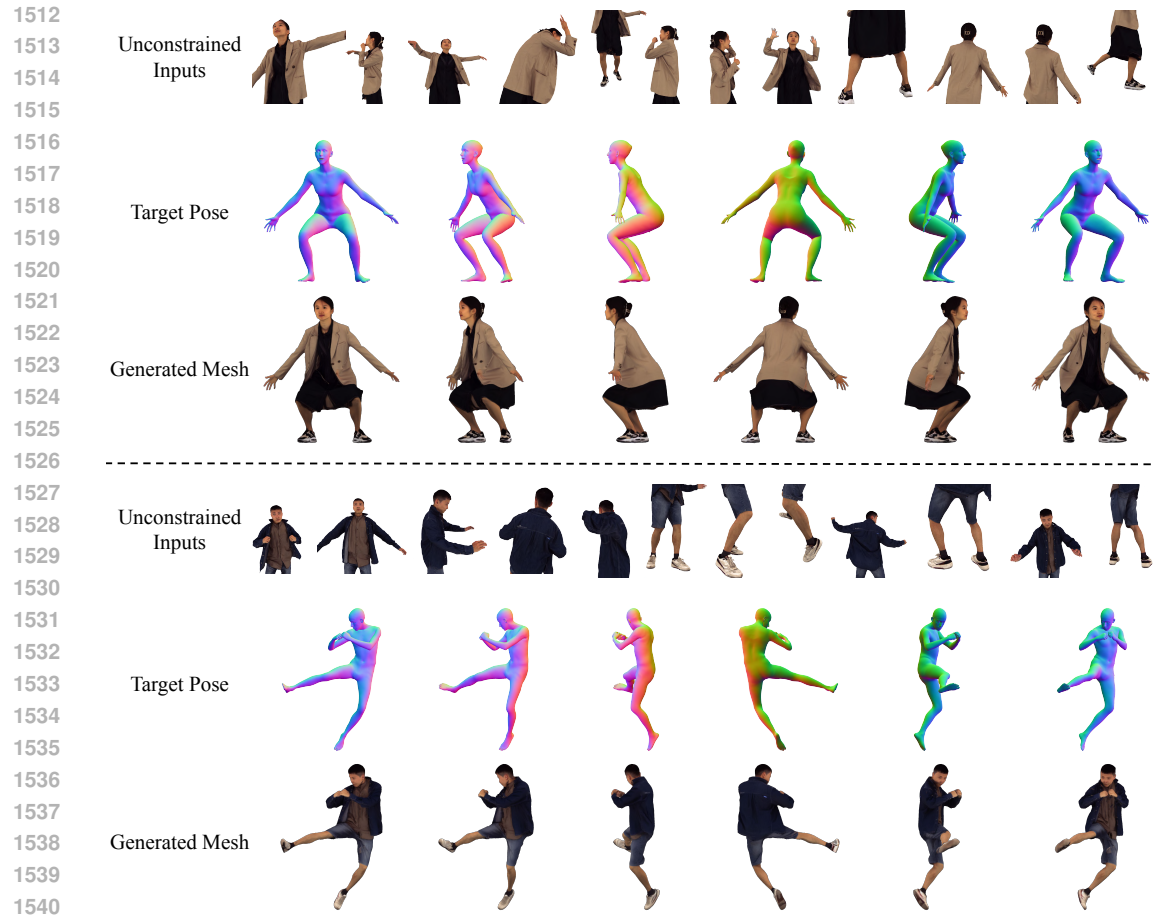


Figure 24: Generation Results with Loose Clothing and Complex Target Pose.

1542
1543
1544
1545
1546
1547
1548
1549
1550
1551
1552
1553
1554
1555
1556
1557
1558
1559
1560
1561
1562
1563
1564
1565

1566
1567

F.3 ANALYSIS OF SHAPE PREDICTOR.

1568
1569

To evaluate whether our shape predictor can regress consistent shape parameters, we assess our shape prediction model using different groups of unconstrained reference inputs from the same identity. As shown in Tab. 10, our method achieves stable shape predictions across all input groups. Since the aggregated pixel-level features from reference inputs may contain information about personal shape characteristics, the multi-view image generation model in UP2You exhibits some degree of robustness to shape variations. However, in extreme cases, more accurate shape predictions can significantly enhance the quality of the final 3D human generation. We evaluate the impact of our shape predictor on the overall inference pipeline of UP2You and find that incorporating the proposed shape predictor leads to measurable improvements in generation quality on the in-the-wild dataset. As demonstrated in Fig. 25, our shape predictor enables more identity-consistent results for individuals with extreme body shapes, while Tab. 11 provides quantitative evidence that the proposed shape predictor improves performance on the in-the-wild dataset.

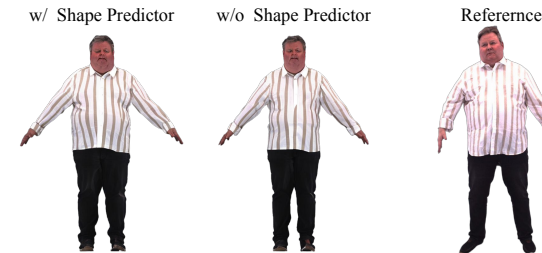
1570
15711572
15731574
15751576
15771578
15791580
15811582
15831584
15851586
15871588
15891590
15911592
1593

Figure 25: **Shape Predictor Helps to Generate More Identity-Consistent Results for People in Extreme Shape.**

1594
15951596
15971598
15991600
16011602
16031604
16051606
16071608
16091610
16111612
16131614
16151616
16171618
1619

	Ref Group A	Ref Group B	Ref Group C
V2V↓ (mm)	7.485	7.503	7.443

Table 10: **Shape prediction consistency on the 4D-Dress dataset.** We input three different groups of 12 reference images of the same person into our shape predictor. The vertex-to-vertex (V2V) error of the predicted results shows stable values with low variance, demonstrating that our shape predictor is robust to unconstrained reference inputs.

	w/ Shape Predictor		w/o Shape Predictor	
	Ours Image	Ours Mesh	Ours Image	Ours Mesh
CLIP- \mathbb{I}^\dagger	0.972	0.971	0.969	0.969
DINO \dagger	0.932	0.916	0.927	0.911

Table 11: **Effects of Shape Predictor on the in-the-wild Dataset.** Generation results with the aid of shape predictor have better performance.

1620
1621

F.4 VISUAL RESULTS WITH DIFFERENT NUMBER OF INPUTS

1622
1623
1624

In UP2You, as more unconstrained photos are provided as input, additional details can be extracted and refined in orthogonal views, thereby improving the reliability of the generated results. We demonstrate this principle through an illustrative example in Fig. 26.

1625

1626

1627

1628

1629

1630

1631

1632

1633

1634

1635

1636

1637

1638

1639

1640

1641

1642

1643

1644

1645

1646

1647

1648

1649

1650

1651

1652

1653

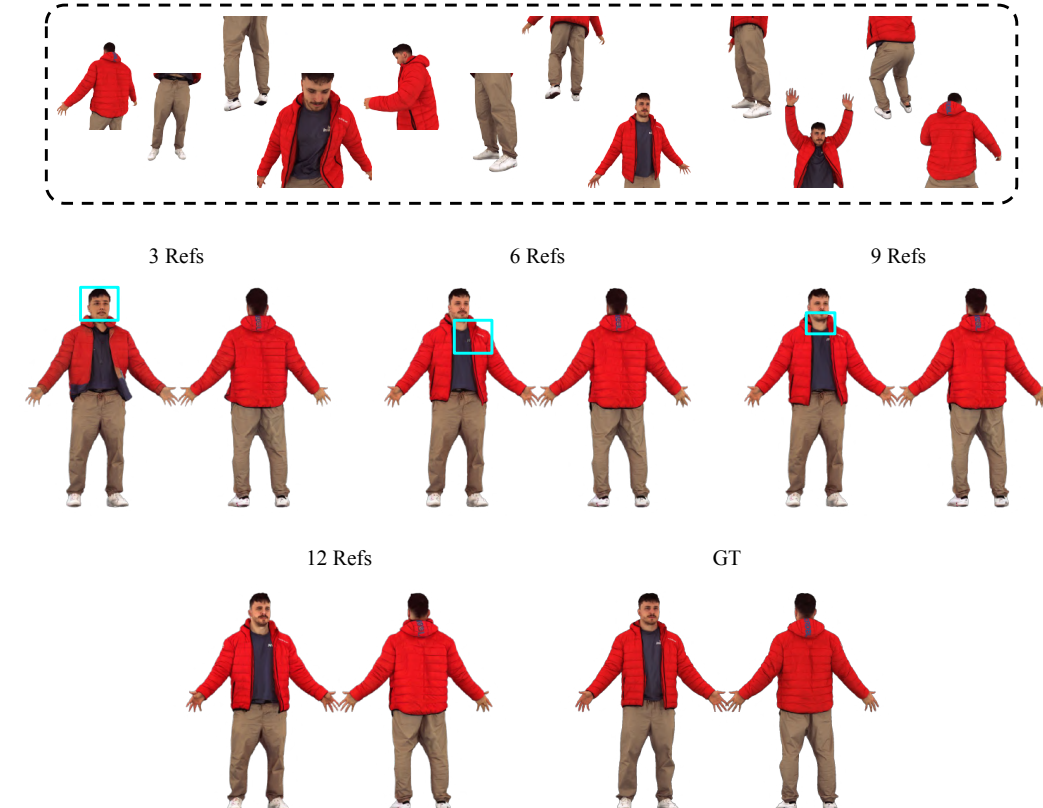


Figure 26: **Generated Multi-View Image Results with Different Number of References.** With more references input, more results are noticed and generated by our model, like facial details and clothing patterns.

1654

1655

1656

1657

1658

1659

1660

1661

1662

1663

1664

1665

1666

1667

1668

1669

1670

1671

1672

1673

1674
1675
G MORE GENERATION RESULTS OF UP2YOU
1676

1677 Figures 27 and 28 present comprehensive generation results of UP2You on two representative cases,
 1678 including the reference images, generated multi-view images and normal maps, as well as the rendered
 1679 images and normal maps after mesh reconstruction. Figure 29 demonstrates that UP2You is robust to
 1680 diverse inputs, performing well even in extreme scenarios such as inputs missing the face, lower body,
 1681 or upper body. Additionally, Figure 30 provides further examples of 3D virtual try-on applications.
 1682
 1683
 1684
 1685
 1686
 1687
 1688
 1689
 1690
 1691
 1692
 1693
 1694
 1695
 1696
 1697
 1698
 1699
 1700
 1701
 1702
 1703
 1704
 1705
 1706
 1707
 1708
 1709
 1710
 1711
 1712
 1713
 1714
 1715
 1716
 1717
 1718
 1719
 1720
 1721
 1722
 1723
 1724
 1725
 1726
 1727

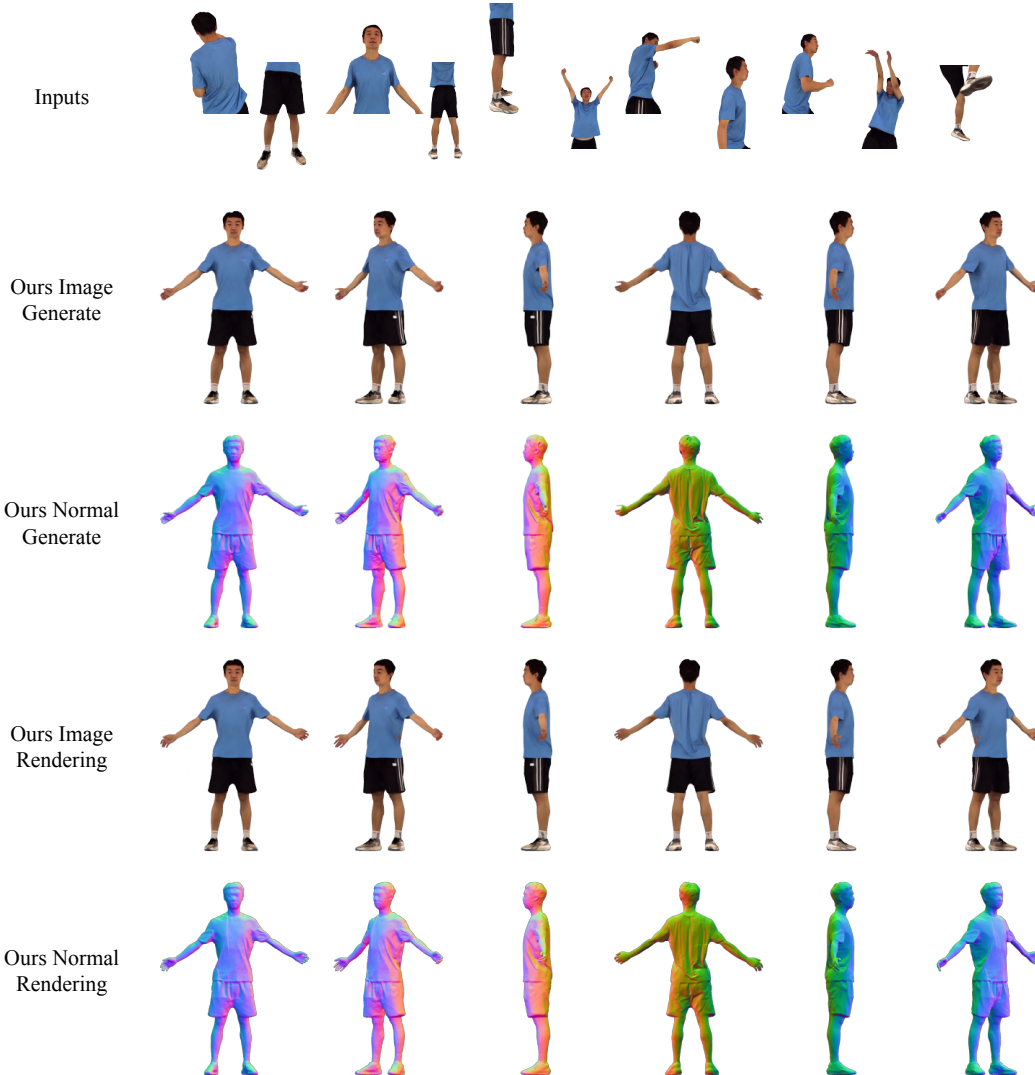
1718
1719
1720
1721
1722
1723
1724
1725
1726
1727





Figure 29: **More Generation Cases with Invisible Parts.** UP2You generates reasonable results with different kinds of invisible scenarios.

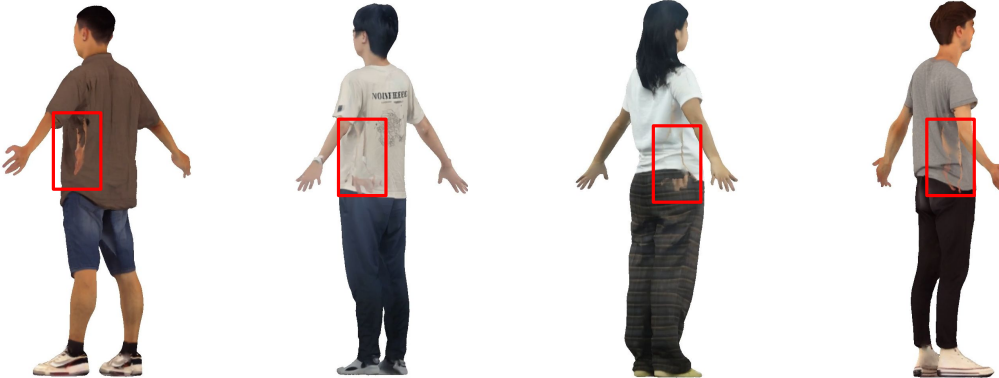


Figure 30: **More examples of 3D Virtual Try-On.**

1890 H LIMITATIONS AND FUTURE WORKS

1891
 1892 While our method shows promising results in generating high-quality 3D human avatars from
 1893 unconstrained photos, there are still some limitations that we plan to address in future work:
 1894

- 1895 • **Dependence on 3D Data for Training:** Our method relies on a dataset of 3D human
 1896 models for training the diffusion model. Acquiring high-quality 3D data can be challenging
 1897 and may limit the diversity of the generated avatars. In future work, we aim to explore
 1898 semi-supervised or unsupervised approaches that can leverage large-scale 2D image or video
 1899 datasets to reduce this dependence on 3D data.
- 1900 • **Texture Misalignment:** Our method generates 6 orthogonal views for mesh reconstruction
 1901 and texturing, which is insufficient for high-quality texture baking. Texture misalignment
 1902 issues may arise in some cases (Fig. 31). In future work, we plan to adopt video generation
 1903 models as the base framework for dense view synthesis to address this limitation.
- 1904 • **Multiple Inference Stages:** When processing in-the-wild photos, our mesh reconstruction
 1905 pipeline involves four sequential stages: shape prediction, multi-view image generation,
 1906 multi-view normal map generation, and mesh reconstruction. This multi-stage inference
 1907 approach slows down the generation process and may introduce cumulative errors. We plan
 1908 to develop a feed-forward model that directly predicts the final results.



1923 Figure 31: **Failure Cases of UP2You.** Since only 6 orthogonal views $\{0^\circ, 45^\circ, 90^\circ, 135^\circ, 180^\circ, 270^\circ\}$ are generated, the backside texture of
 1924 generated humans is lacking in guidance, making the problem of texture misalignment.